Published in final edited form as:

Structure. 2021 July 01; 29(7): 664–678.e6. doi:10.1016/j.str.2021.01.003.

Interplay between hevin, SPARC, and MDGAs: modulators of neurexin-neuroligin trans-synaptic bridges.

Shanghua Fan[1,2], **Shanti Pal Gangwar**[1,2], **Mischa Machius**[1,2], **Gabby Rudenko**[1,2,*]

[1]Dept. of Pharmacology and Toxicology, University of Texas Medical Branch, Galveston TX, 77555, USA

[2]Sealy Center for Structural Biology and Molecular Biophysics, University of Texas Medical Branch, Galveston TX, 77555, USA

Summary

Hevin is secreted by astrocytes and its synaptogenic effects are antagonized by related protein, SPARC. Hevin stabilizes neurexin-neuroligin trans-synaptic bridges *in vivo.* A third protein, membrane-tethered MDGA, blocks these bridges. Here, we reveal the molecular underpinnings of a regulatory network formed by this trio of proteins. The hevin FS-EC structure differs from SPARC, in that the EC domain appears rearranged around a conserved core. The FS domain is structurally conserved and it houses nanomolar-affinity binding sites for neurexin and neuroligin. SPARC also binds neurexin and neuroligin, competing with hevin, so its antagonist action is rooted in its short N-terminal region. Strikingly, the hevin FS domain competes with MDGA for an overlapping binding site on neuroligin, while the hevin EC domain binds the extracellular matrix protein collagen (like SPARC), so that this trio of proteins can couple neurexin-neuroligin trans-synaptic bridges and the extracellular matrix, impacting synapse formation and ultimately neural circuits.

Graphical Abstract

[*]To whom correspondence should be addressed: G. Rudenko, University of Texas Medical Branch, 301 University Blvd. Galveston, TX 77555, USA, Tel.: (409) 772-6292, garudenk@utmb.edu.

Author Contributions: S.F. and G.R. designed the study and wrote the paper. S.F. and G.R. designed the constructs used for the expression of proteins. S.F. and S.P.G. purified proteins. S.F. carried out the crystallizations. S.F. and M.M. performed the structure determination and structural analyses. S.F. performed the biochemical and biophysical characterization of hevin, SPARC and their partners. All authors reviewed the results and approved the final version of the manuscript.

Declaration of Interests: The authors declare no competing interests.

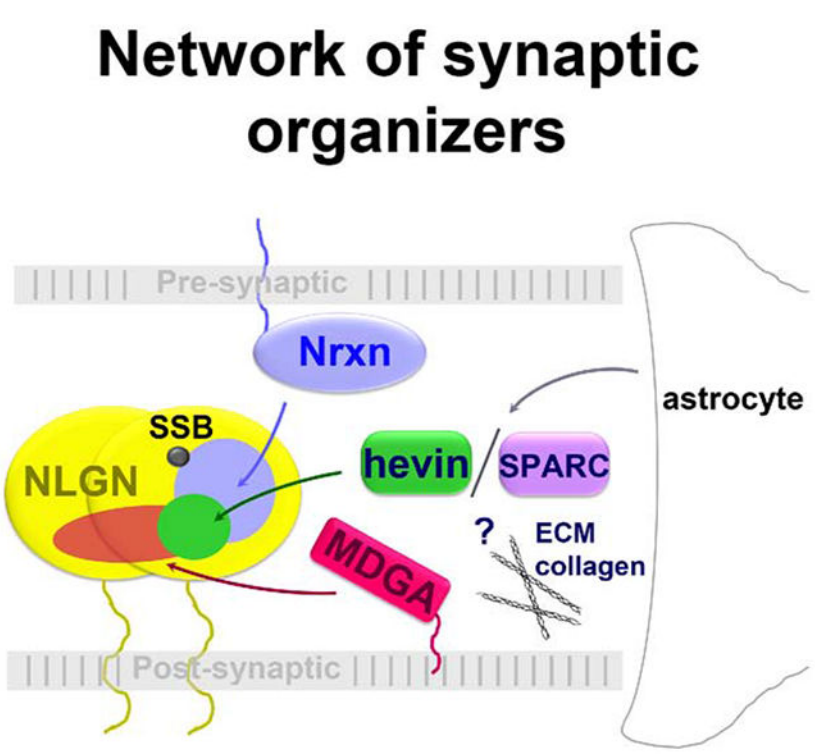

In brief (eTOC blurb)

Neuroligins and neurexins form trans-synaptic bridges that promote synapse development. Fan et al. reveal the molecular mechanism of hevin action, a secreted positive regulator of this trans-synaptic bridge, and unveil unexpected interplay with other regulators, SPARC and MDGA.

Keywords

hevin; SPARC; neurexins; neuroligins; MDGAs; synaptic organizer; adhesion molecule; matricellular protein; collagen; protein structure

Introduction

Hevin (high endothelial venule protein), also known as SPARCL1 (SPARC-like 1, SC1, secreted protein acidic and rich in cysteine-like 1), is a secreted matricellular protein that promotes the formation and maintenance of neural circuits in mammalian brain by altering synaptic connections between neurons as well as impacting the position of neurons as they migrate (Allen and Eroglu, 2017; Ferrer-Ferrer and Dityatev, 2018; Jones and Bouvier, 2014; Yuzaki, 2018). Hevin is composed of an N-terminal thread-like, flexible acidic region and a C-terminal globular region containing a follistatin-like (FS) domain and an EF-hand calcium-binding (EC) domain (Hambrock et al., 2003). The FS-EC tandem has ~62% sequence identity to the matricellular protein, SPARC (secreted protein acidic and rich in cysteine), a much smaller protein with a very short N-terminal region that is not conserved with hevin (Bradshaw, 2012; Girard and Springer, 1995; Murphy-Ullrich and Sage, 2014). Proteins that induce and/or maintain synapses are an important focal point of study because

they are increasingly linked to neuropsychiatric disorders (Südhof, 2017), but for many, including hevin, relatively little is known about their molecular mechanisms.

Hevin and SPARC have both similar as well as opposing biological functions in the brain. Hevin stimulates excitatory synapse formation (Gan and Südhof, 2019, 2020; Kucukdereli et al., 2011). Its action is important to generate refined neural circuits; for instance, hevin secreted by astrocytes promotes and stabilizes thalamocortical excitatory synapses in the developing mouse visual cortex, strengthening the connections between the two brain regions, at the cost of the intracortical excitatory connections which are eliminated (Kucukdereli et al., 2011; Risher et al., 2014; Singh et al., 2016). SPARC also impacts synapse formation, albeit differently than hevin (Bradshaw, 2012; Murphy-Ullrich and Sage, 2014). SPARC lacks the ability to induce synaptogenesis and it blocks hevin action (Kucukdereli et al., 2011). Interestingly, a fragment of hevin, SLF (SPARC-like fragment), that encompasses the FS and EC domains just like SPARC, is also not synaptogenic and likewise blocks hevin-induced synapse formation (Kucukdereli et al., 2011). SPARC triggers a cell-autonomous program of synapse elimination in cholinergic neurons (López-Murcia et al., 2015), although in single-cell cholinergic neuron microcultures it increases the formation of autapses (i.e., synapses from one neuron onto itself) (Albrecht et al., 2012). SPARC also regulates the efficiency of synaptic communication in developing hippocampus by controlling the number of AMPA-receptor subunits at synapses via a β3-integrin mediated mechanism, while hevin does not (Jones et al., 2011). However, both hevin and SPARC alter neurite outgrowth (thus influencing neuron morphology), as well as neuronal migration and connectivities during postnatal development (López-Murcia et al., 2015; Vincent et al., 2008), perhaps via interactions with the extracellular matrix. SPARC has a well-described role in extracellular matrix assembly through its ability to bind collagen, which has been elucidated by structural studies. Whether hevin binds collagen as well is unclear (Bradshaw, 2012; Hohenester et al., 2008; Murphy-Ullrich and Sage, 2014). In the brain, hevin and SPARC show characteristic expression patterns that are temporally and spatially regulated, placing these molecules in highly strategic positions to modulate neural circuit formation and maintenance during development and beyond. Throughout postnatal development, hevin is abundantly expressed in astrocytes and in subsets of projection neurons, escalating to high levels during a peak period of synaptic remodeling (Lively and Brown, 2008a; Lloyd-Burton and Roskams, 2012; Mendis et al., 1996; Risher et al., 2014). However, hevin is also strongly expressed in many regions in adult brain in most astrocytes, and also, in select populations of inhibitory and excitatory neurons (Hashimoto et al., 2016; Lively et al., 2007; Lloyd-Burton and Roskams, 2012; Mendis et al., 1996; Mongrédien et al., 2019; Risher et al., 2014). Like hevin, SPARC is broadly expressed during development in glial cells and radial glia (progenitor cells that additionally function as guide cells along which neurons migrate) (Vincent et al., 2008), but in adult CNS, SPARC is expressed only in very limited regions by astrocytes and microglia but not neurons (Lloyd-Burton and Roskams, 2012; Mendis et al., 1995; Mongrédien et al., 2019; Vincent et al., 2008). Given the high sequence identity, the striking biological differences between hevin and SPARC remain puzzling, especially as they also seem to share certain functions, as described above, and this dichotomy is important given the characteristic temporal and spatial expression patterns of hevin and SPARC.

The molecular mechanisms of hevin and SPARC actions in the brain are unclear. *In vivo*, hevin appears to promote the interaction between two families of synaptic organizers, the post-synaptic neuroligins and the pre-synaptic neurexins, and it is proposed to join them together in trans-synaptic bridges that span and stabilize synaptic junctions (Singh et al., 2016). Neurexin-neuroligin complexes are among the most extensively studied trans-synaptic bridges and are particularly notable because of their diverse composition and their links to neuropsychiatric disorders (Rudenko, 2019; Südhof, 2017). In humans, five neuroligin (NLGN) genes encode proteins containing a membrane-tethered, dimeric ectodomain with a cholinesterase-like fold, which is variably diversified through alternative splicing at two splice insert sites, site A (SSA) and site B (SSB) (Bemben et al., 2015; Südhof, 2017). Similarly, three neurexin (NRXN) genes generate membrane-tethered proteins with highly variable extracellular regions. α-Neurexins contain 6 LNS (laminin G, neurexin, sex-hormone binding globule) domains and 3 EGF (epidermal growth factor)-like repeats, while β-neurexins are composed of only a single LNS domain. Neurexins are also extensively diversified at alternative splice sites (SS1–6) (Südhof, 2017). Contrasting hevin as a promoter of neurexin-neuroligin trans-synaptic bridges, the MDGA (MAM domain-containing glycosylphosphatidylinositol anchor protein) family of synaptic organizers (composed of six immunoglobulin (Ig) domains, one fibronectin III and one MAM (meprin, A5 protein, PTPμ) domain tethered to the post-synaptic membrane) destabilizes neurexin-neuroligin trans-synaptic bridges. They do so by binding to neuroligin and blocking the recruitment of neurexin (Elegheert et al., 2017; Gangwar et al., 2017; Kim et al., 2017). But it is not known if, and how, MDGAs, hevin and SPARC interplay. Furthermore, recent studies have drawn into question whether hevin interacts with the neurexin-neuroligin trans-synaptic bridge directly, or even at all, and whether hevin's synaptogenic effect involves these trans-synaptic bridges (Elegheert et al., 2017; Gan and Südhof, 2020). For SPARC, it is also not known if it binds neurexin and/or neuroligin. So, while hevin and SPARC are strategically positioned to impact neural circuitries in developing and mature brain, whether they carry out synergistic, opposing, or indeed independent functions is not clear, in part due to the lack of structure-function relationships.

Here, we establish interplay between the trio of proteins, hevin, SPARC, and MDGA, and elucidate the molecular mechanism. First, we show that the hevin FS-EC tandem features striking structural differences compared to SPARC, predominantly in the EC domain. We show that hevin and SPARC are both able to bind to neuroligin and neurexins, suggesting that they can act in concert to regulate neurexin-neuroligin trans-synaptic bridges. We further show that the hevin FS domain, which is structurally conserved in SPARC, is sufficient to bind both neuroligin and neurexin with nanomolar affinity. Importantly, we find that hevin and MDGAs occupy overlapping binding sites on neuroligin explaining how they compete with each other for neuroligin binding. Finally, we show that hevin, like SPARC, binds to collagen in solution, but we do not observe the same collagen-binding site as in the SPARC structure. Collectively, our results establish that hevin and SPARC can take part in a complex symphony of competing protein interactions, vying for synaptic organizers as well as interacting with extracellular matrix components. Key structural features provide rationales for both the shared and fundamentally different biological roles of hevin and SPARC in the brain.

Results

Hevin FS-EC structure

Hevin FS-EC and fragments were produced using baculovirus-mediated over-expression (Figures 1A and S1A). Because attempts to solve the hevin FS-EC X-ray crystal structure by molecular replacement using SPARC as a search model (PDB: 1BMO and 2V53) were unsuccessful, the Ca^{2+} ions in the EF-hands were substituted with holmium and the hevin crystal structure determined through single isomorphous replacement with anomalous scattering (SIRAS) phasing (Table 1). The final model of hevin FS-EC was refined using data to 2.27 Å resolution (R_{work}=18.9%; R_{free}=24.1%) (Table 1). The hevin FS domain (V^{430}-C^{509}) is composed of an EGF-like repeat (V^{430}-Q^{457}) containing two disulfide bonds as well as a Kazal domain (D^{458}-K^{509}) containing a mixed α/β fold stabilized by three disulfide bonds (Figure 1B). The EC domain (C^{515}-F^{664}) houses two canonical helix-loop-helix EF-hands (EF1 and EF2) that each contain a Ca^{2+}-binding site with seven-oxygen coordination; the EF-hands are connected by a short helical turn ($D^{517}FEV^{520}$) that packs adjacent to an elongated bundle of helices (αA, αBC, αC) (Figures 1B and 1C). A disulfide bond between C^{634} and C^{650} stabilizes EF2, with a second disulfide bond between C^{515} and C^{626} connecting EF1 to the linker (K^{510}-T^{514}) between the FS and EC domains. A large cleft separates the FS and EC domains. The interface between the two domains is small (~200 $Å^2$) and contains only a few residues from strand β5 of the FS domain and from helix αF and the loop connecting the two EF-hands in the EC domain (Figure 1B). Two hevin molecules (mol A and mol B) embrace each other tightly in the asymmetric unit of the crystal structure so that helices αA and αC from the EC domain of mol B interact with the EC domain and Kazal subdomain of the neighboring mol A, with Y^{539} from helix αA fitting like a key in the cleft; likewise, helices αA, and αBC from the EC domain of mol A insert into mol B in a similar manner (Figures 1D and S2A). Because mol A and mol B are stabilized by an additional Ca^{2+}-ion binding between them, and the monomers adopt similarly ‘open’ configurations between the FS and EC domains (Figures S2A and S2B), we tested whether the hevin FS-EC tandem behaves as a dimer in solution. However, in analytical ultracentrifugation (AUC), size exclusion chromatography (SEC) and cross-linking studies, hevin FS-EC (hevin_C2) is monomeric in solution, even in an acidic buffer similar to that used for crystallization and/or in presence of increasing amounts of Ca^{2+} (Figures S2C, S2D and S2E). To gauge whether the FS and EC domains, which are kept apart in the crystal structure, are able to associate in solution, we used SEC and demonstrated that the isolated FS (hevin_C5) and EC (hevin_C6) domains do not associate in solution, at least not without the linker between the two domains (Figures 1E). Taken together, the hevin FS-EC tandem forms an elongated structure that exists as a monomer in solution, and the two domains appear independent of each other, suggesting that they can function autonomously.

Hevin and SPARC FS-EC structures are fundamentally different

The hevin FS-EC and SPARC FS-EC (Hohenester et al., 1997) structures feature striking differences despite their high level of sequence identity (55% for the FS domain and 63.2% for the EC domain, respectively) (Figures 2A and 2B). Though the hevin and SPARC FS domain have similar folds (root-mean-square deviation (rmsd) of 1.2 Å for 79 C^{α}

superimposable residues) (Figure 2C, left), the hevin FS domain is rotated away from the EC domain by ~40° into an 'open' form compared to SPARC, 1BMO (Figure 2C, right). Consequently, the hevin FS-EC interface is smaller (~200 $Å^2$) compared to the SPARC FS-EC interface (~370 $Å^2$) even though most residues at the interface are conserved (Figure 2A). Unexpectedly, the hevin and SPARC EC domains show dramatic structural differences; only 94 C^{α} residues out of 128 (hevin) and 150 (SPARC) residues observed in the respective crystal structures superimpose with an rmsd of 1.5 Å (Figure 2C, right). The two EF hands form a structurally conserved core, differing only in their connecting segment (Figure 2D). However, the region between the FS domain and EF-hand tandem, I^{512}-N^{584} (I^{135}-N^{223} in SPARC) is completely reorganized so that helices αA', αA, αBC and αC (here referred to as 'variable helices') now point away from the EF hands (Figure 2D). Despite the high sequence identity (45 residues out of the 73-residue stretch I^{512}-N^{584}), the region containing these variable helices has completely rearranged: the single, contiguous helix αA in SPARC is broken up in hevin into two kinked helices (αA'-αA); helix αB in hevin is disordered; and helices αBC and αC adopt a different fold (Figure 2D). Interestingly, in SPARC, helices αA, αB, and αC play an important role in maintaining high-affinity Ca^{2+}-binding of the EF-hand pair, in particular helix αA, a long amphiphilic helix that inserts into the hydrophobic core of the EF-hand pair (Hohenester et al., 1996). Thus, despite significant sequence conservation, the hevin EC domain is structurally distinct from the SPARC counterpart, while the FS domains are similar, at least as observed in their crystalline environments.

Hevin binds neuroligins

To investigate if and how hevin interacts with the extracellular domains of NLGNs, we tested the binding of a panel of hevin fragments to different NLGN splice forms (Figure 3A); full length human hevin (hevin_C1) did not express well, so that this construct was not further pursued. TAMRA(TMR)-labeled hevin FS-EC (hevin_C2) interacts with NLGN1 and NLGN2 with similar affinity in solution in a fluorescence polarization (FP) binding assay (dissociation constant, K_D 60-116 nM), regardless of whether the SSA or SSB inserts are present (Figure 3B). To further delineate the minimal region of hevin required for neuroligin binding, we tested a series of hevin fragments for their binding to NLGN2(+A) using surface plasmon resonance (SPR) (Figure 3C). Strikingly, the FS domain (hevin_C5) bound to NLGN2(+A) with ~12x higher affinity (K_D 60.4 ± 3.6 nM) compared to the EC domain (hevin_C6) (K_D 705.0 ± 41.0 nM), suggesting that the hevin FS domain contains the key residues for neuroligin binding, results that we corroborated qualitatively with our FP assay (Figure 3D). In comparison, under similar experimental conditions, binding of neurexin 1α (n1α) L1L6 to NLGN2(+A) is about 15 times tighter (K_D 3.8 ± 0.6 nM) (Figure 3C). Taken together, these data suggest that the FS domain contains the key residues for binding of hevin to neuroligins.

Hevin binds neurexin

To investigate if hevin interacts with neurexins, as well, and by which mechanism, we tested the binding of the hevin FS domain to neurexin 1α (n1α) in FP assays (Figures 4A and 4B). The interaction between the hevin FS and neurexin 1α is Ca^{2+}-dependent, suggesting that the 'hyper-variable' surface of one or more of the neurexin LNS domains, which house a centrally-located Ca^{2+}-binding site, is involved (Rudenko et al., 1999). Furthermore, n1α

L1L6, n1α L5L6, and n1α L1L5 all bind the hevin FS domain similarly in a Ca^{2+}-dependent reaction, while n1α L2L3 does not, suggesting that the L5 domain of neurexin 1α (the common denominator) contains a critical binding site for hevin interaction (Figures 4A and 4B). Interestingly, a complex pre-formed between the TMR-labeled hevin FS domain and n1α L5L6 recruits NLGN2(+A) and NLGN1(−A,+B) similarly in solution in a Ca^{2+}-dependent interaction, while n1α L2L3 mixed with the TMR-labeled hevin FS domain (which do not bind well) does not, suggesting that the hevin FS domain alone is sufficient to form a tripartite complex with neurexin and neuroligin (Figures 4C and 4D). Taken together, these data suggest that hevin interacts directly with neurexins in solution, likely requiring the FS domain of hevin, and the α-neurexin specific L5 domain.

SPARC binds neuroligin and neurexin

Given that SPARC antagonizes hevin action, working perhaps as a competitor (Kucukdereli et al., 2011), we tested whether SPARC could also bind neuroligin and neurexin (Figure 5). In solution, full-length SPARC (SPARC_C1) and the SPARC FS-EC domains (SPARC_C2) bind to NLGN2(+A) with similar affinity (K_D ~37-96 nM) as the hevin FS-EC tandem (hevin_C2) (K_D ~55 nM) in an FP-based assay (Figures 5A and 5B). To gain more quantitative insight, we tested the interaction of SPARC with NLGN2(+A) by SPR, revealing that full-length SPARC (SPARC_C1) and SPARC FS-EC (SPARC_C2) bind NLGN2(+A) similarly well (K_D 115.5 ± 21.5 nM and K_D 300 ± 10 nM, respectively) (Figure 5C) and similar to hevin FS-EC (hevin_C2; K_D 118.5 ± 17.5 nM) (refer back Figure 3C) consistent with results from our FP-assays. Furthermore, in a competition experiment, SPARC and SPARC FS-EC both disrupted the pre-formed hevin FS:NLGN2(+A) complex as effectively as hevin FS-EC (Figure 5D). Given the high structural similarity between the hevin and SPARC FS domains, unlike their EC domains, we hypothesized that SPARC might also bind to neurexins. We thus tested the binding of a panel of neurexin 1α fragments to SPARC in an FP assay and revealed that SPARC has a very similar binding profile as hevin (Figure 5E). Taken together, SPARC binds NLGN2(+A) in solution with an affinity that is comparable to that of hevin, positioning it to compete with hevin for binding to neuroligins at synapses. SPARC also binds to neurexin 1α in a Ca^{2+}-dependent manner, similar to hevin, suggesting that hevin and SPARC can compete for neurexins, as well, when both are present.

Hevin competes with MDGA for neuroligin

Unlike hevin, which promotes the formation of neurexin-neuroligin trans-synaptic bridges, the synaptic organizers MDGA1 and MDGA2 inhibit this interaction (Connor et al., 2016; Lee et al., 2013; Pettem et al., 2013). The MDGA1 Ig1 and Ig2 domains straddle the NLGN2 dimer, with Ig1 binding to one NLGN2 monomer sterically blocking the neurexin binding site, while Ig2 binds to the other NLGN2 monomer stabilizing the interaction (Elegheert et al., 2017; Gangwar et al., 2017; Kim et al., 2017) (Figure 6A). To assess whether hevin and MDGAs compete with each other for neuroligin binding, we tested if validated mutations located on the surface of NLGN2 that disrupt the interaction with MDGA1 Ig1-Ig2 (Gangwar et al., 2017) affect the binding of hevin as well (Figure 6A). Indeed, the hevin FS domain (hevin_C5) binds such mutants very weakly (NLGN2 Mut1, Mut3, and Mut4), while it binds readily to wild-type NLGN2(+A) and NLGN2 Mut2 (a

mutant that does not interfere with MDGA1 binding); therefore, the hevin FS domain binds to the same surface region on NLGN2 as MDGA1 Ig1 does (Figure 6B). Indeed, MDGA1 Ig1-Ig2 (MDGA1_C8) disrupts the hevin FS:NLGN2 complex in competition experiments (Figure 6C). Likewise, a mutant MDGA1 Ig1-Ig2 engineered to have weakened affinity for NLGN2 (MDGA1_C8 Mut4; $R^{105}A$, $Y^{107}A$, $R^{123}A$, $F^{154}A$, $R^{156}A$, $Y^{187}A$) (Gangwar et al., 2017) disrupts the hevin FS:NLGN2 complex also less efficiently (Figure 6C). However, the hevin FS domain does not appear to readily interact with MDGA1 directly (Fig. S5). Hence, the hevin FS domain and MDGA1 Ig1 share overlapping binding sites on NLGN2 that co-localize with the binding site for neurexins, putting them in position to compete with each other.

Hevin binds collagen V

An important biological function of SPARC is to bind to collagen in order to regulate the interaction of collagen with cell surface receptors and the assembly of collagen into fibrils (Bradshaw, 2009). SPARC binds collagen I, II, III, IV and V in a Ca^{2+}-dependent manner with relatively low affinity (K_D ~1-4 μM) but proteolytic cleavage of helix αC by matrix metalloproteinases (MMPs) or engineered removal of αC (V^{213}ELLARDF^{220}, designated V^{196}ELLARDF^{203} in PDB: 2v53 and 1nub) increase the affinity ~10x (Bradshaw, 2009; Hohenester et al., 2008; Maurer et al., 1997; Sasaki et al., 1998). Low-resolution electron microscopy studies have suggested that hevin binds collagen as well (Hambrock et al., 2003). However, while SPARC-null mice have decreased levels of fibrillary collagen, puzzlingly, hevin-null mice do not, and SPARC and hevin impact the assembly of collagen fibers differently in *in-vitro* studies (Bradshaw, 2012; Giudici et al., 2008; Maurer et al., 1997; Sullivan et al., 2006). The ability of hevin to bind collagen in the brain would have important consequences, because hevin could tether neurexin-neuroligin trans-synaptic bridges to the extracellular matrix through this interaction, and hevin secreted by astrocytes could then further stabilize synapses. Based on the structure of the complex between SPARC and a collagen III tripeptide, there are 13 key SPARC residues that bind collagen (Hohenester et al., 2008). Hevin shares high sequence identity with the collagen-binding region in SPARC (9 out of these 13 residues are identical, and 3 are semi-conserved) (Figure 7A). The SPARC EC domain clamps a trimeric collagen III peptide into a crevasse between helix αA and the loop connecting the αE and αF helices, burying F^{23} of the collagen trailing strand into a deep pocket (Figure 7B) (Hohenester et al., 2008) (PDB: 2v53). Strikingly, in our hevin structure, this region is organized differently with αA rotating away from loop(αE-αF) and broken up into two helices, αA' and αA, so that F^{523}, R^{526}, M^{527}, W^{530} (the counterparts for the collagen-binding residues in SPARC) point towards the solvent (Figure 7C). Interestingly, in the collagen-bound form of SPARC, the FS-EC tandem adopts an 'open' conformation that is almost identical to that seen in hevin, and the FS/EC interface is similar in size (175 $Å^2$) as well (Figure 7D). Given the structural differences in the EC domain between hevin and SPARC, in particular those residues involved in collagen binding in SPARC, it is uncertain if hevin is capable of binding collagen. To test whether hevin binds collagen as well, we used FP and SPR to assess the interaction between the hevin EC domain (hevin_C6) or the hevin FS domain (hevin_C5) with human collagen V, a fibrillar collagen that is expressed in very specific regions in the brain, including the isocortex, cerebellum and hippocampus (Lein et al., 2007), as well as outside the brain. Remarkably,

the hevin EC domain bound collagen V efficiently with low micromolar affinity, in a Ca^{2+}-dependent fashion, while the hevin FS domain did not, suggesting that hevin can interact with specific collagens in the brain extracellular matrix (Figures 7E and 7F). Thus, although hevin apparently lacks a collagen binding site as organized in SPARC, it nonetheless binds collagen V with micromolar affinity. In future, it will be important to determine whether hevin couples neurexin-neuroligin trans-synaptic bridges to the extracellular matrix via collagen binding.

Discussion

Hevin is strategically positioned to play an important role in establishing and remodeling neuronal connections, because it is secreted not only in developing, but also, in mature brain (Allen and Eroglu, 2017; Jones and Bouvier, 2014; Mongrédien et al., 2019). SPARC, on the other hand, is expressed at high levels in brain during development but in adult only in a small number of select brain regions as well (Allen and Eroglu, 2017; Jones and Bouvier, 2014; Mongrédien et al., 2019). SPARC can antagonize hevin action, strikingly, negatively impacting synapse number and function (Allen and Eroglu, 2017; Kucukdereli et al., 2011). Hevin is proposed to promote the formation of neurexin-neuroligin trans-synaptic bridges (Singh et al., 2016), in contrast to MDGAs (Connor et al., 2016; Lee et al., 2013; Pettem et al., 2013), while the effect of SPARC on neurexin-neuroligin trans-synaptic bridges has not been established. Here, we demonstrate that hevin and SPARC can interact directly with neurexins and neuroligins in solution and reveal key structure-function relationships that explain their apparent opposing, as well as shared biological functions, and we demonstrate their direct molecular interplay with MDGAs through a competitive mechanism.

Hevin and SPARC FS-EC structures share both striking differences as well as similar features. ***First***, the EC domains are structurally different due to the helices that flank the two highly conserved EF-hands (αA, αB, and αC in SPARC) rotating outwards in hevin and undergoing a virtually complete rearrangement (the ‘variable’ helices αA’, αA, αBC, and αC) compared with SPARC. By contrast, the FS domains are structurally very similar (Figure 7G). Though very different in shape, the surfaces of the hevin and SPARC EC domains are nevertheless highly conserved, paralleling the extent of surface conservation seen for the structurally very similar FS domains (Figures 2B, S3 and S4). ***Second***, as a consequence of the dramatic rearrangement of the ‘variable’ helices (in particular αA), a collagen binding site found in SPARC, is fundamentally rearranged in hevin. Of note, while one side of the collagen binding cleft is altered by the rearrangement of helix αA, the other side composed of loop(αE-αF), however, still resembles the collagen-bound counterpart in SPARC which moves outward to accommodate the fibril (Hohenester et al., 2008) (see PDB: 2v53 and 1nub). We show that hevin nevertheless binds collagen V with low micromolar affinity, which suggests that hevin either contains a novel collagen-binding site or that the EC domain can rearrange to form a collagen-binding site as observed in SPARC. ***Third***, the relative position of the FS domain with respect to the EC domain is ‘open’ in hevin, while it is ‘closed’ in SPARC in a comparable ligand free-form. Interestingly, when SPARC binds to a collagen peptide, the FS domain is seen to adopt an ‘open’ configuration very similar to ligand-free hevin (Hohenester et al., 2008), suggesting that the relative orientation of the FS and EC domains can vary in solution, and perhaps is further impacted by protein partner

binding. Together, our data suggest that hevin and SPARC contain structural features that are conserved (the FS domain), drastically different (the EC domain), and plastic (the relative orientation of the FS and EC domains) and that these may rearrange in order to interact with an array of different protein partners as they carry out various functions. It will be important in future work to validate these structural findings using orthogonal techniques in order to assess the extent to which crystal packing forces can influence the architecture and shape of these proteins.

Hevin and SPARC take part in a network of synaptic proteins that vie for each other's interactions and target neurexin-neuroligin trans-synaptic bridges (Figure 8). ***First***, we show that the hevin FS domain is sufficient for binding to neuroligins and neurexins. These results are consistent with 1) cell-based studies in which a fragment of mouse hevin (F^{350}-G^{459}) containing a 68 amino-acid N-terminal stretch (F^{350}-G^{417}) and a piece of the FS domain (S^{418}-G^{459}, which spans the EGF repeat and strand β3) bound to NLGNs and n1α, and induced synaptogenesis; and 2) co-immunoprecipitation studies in which the N-terminal portion of mouse hevin (I^{17}-G^{417}, terminating before the FS domain) did not bind NLGNs or neurexins, nor did it efficiently induce pre- or post-synaptic clustering or synaptogenesis (Singh et al., 2016). Puzzlingly, however, in those studies the C-terminal portion of hevin containing the FS-EC domain (F^{350}–I^{650} in mouse) immunoprecipitated neuroligins and induced post-synaptic clustering, but it did not interact with neurexins (Singh et al., 2016). Significantly, neither the N-terminal nor the C-terminal portions of hevin, alone, were sufficient to induce synaptogenesis (Singh et al., 2016). Our findings here are consistent with a model whereby the FS domain of hevin recruits the neurexin-neuroligin trans-synaptic bridge, while the N-terminal region of hevin (not found in SPARC) recruits additional partners that are necessary to promote synaptogenesis. Our data are also consistent with recent findings that hevin can have synaptogenic activity independent of neurexin-neuroligin trans-synaptic bridges (Gan and Südhof, 2020), as additional partners recruited to the hevin N-terminal region could promote synapse formation independent of neurexins and neuroligins in some neural circuits and brain regions. ***Second***, our finding that SPARC is able to bind neuroligins and neurexins is important because SPARC and SLF (a proteolytic fragment of hevin generated *in vivo* containing the FS-EC region) do not induce synaptogenesis, though they both block hevin-induced synapse formation (Kucukdereli et al., 2011). SPARC thus appears to be able to directly compete with hevin for binding to neurexin and neuroligin *in vivo* but cannot efficiently induce synapse formation, likely because it lacks the required N-terminal region that is present in hevin. Therefore, (activity-dependent) proteolytic release of the hevin SLF fragment or secretion of SPARC could remodel synaptic connections, e.g., leading to their elimination. Indeed, SPARC triggers the elimination of cholinergic synapses via a cell-autonomous program, though the exact molecular mechanism is unclear (López-Murcia et al., 2015). ***Third***, we find that the hevin FS domain interacts with neurexins in a Ca^{2+}-dependent manner that involves at least the presence of the n1α L5 domain. This observation is consistent with previous co-immunoprecipitation studies showing that hevin does not bind n1β, which contains a sole module identical to neurexin n1α L6 (Singh et al., 2016). Hevin may work in a sandwich between both neurexin and neuroligins, binding the proteins with nanomolar affinity. In doing so, by binding to n1α L5 as opposed to n1α L6, hevin would allow neurexins and

neuroligins to interact in a way that bypasses the prototypical splice insert-dependent mechanism that is shaped by the steric incompatibility of splice insert SSB in NLGN1 and domains found in α-neurexins (Chen et al., 2011; Rudenko, 2019; Singh et al., 2016; Südhof, 2017). In agreement, when hevin levels exceed a threshold (~100 nM), it actually starts to inhibit tri-partite complex formation with neurexins and neuroligins (Singh et al., 2016), as would be expected for a protein that binds in between two other proteins gluing them together because an excess would saturate the binding sites and prevent hevin bridging two molecules. Also, SPARC is estimated to reach low nanomolar concentrations in the neuroglial space (Albrecht et al., 2012), consistent with its nanomolar affinities for neurexin and neuroligin that we observed biochemically. In future, it will be critical to obtain structural information on tri-partite complexes containing the full-length neurexin 1α, neuroligin and hevin or SPARC. ***Fourth***, we show that hevin competes with MDGAs for binding to neuroligins. MDGA1 and MDGA2 inhibit the formation of neurexin-neuroligin trans-synaptic bridges by binding to NLGNs and blocking the neurexin binding site (Connor et al., 2019; Elegheert et al., 2017; Gangwar et al., 2017; Kim et al., 2017). We show that hevin binds both NLGN1 and NLGN2 (indeed they share extensive sequence conservation on their surface), and that the hevin FS binding site on NLGN2 overlaps with that of MDGA1 Ig1 (and likely that from MDGA2 Ig1 as well based on sequence similarity) (Gangwar et al., 2017; Singh et al., 2016) (Figures 3b and 6). While hevin has a well-described role at excitatory synapses where it encounters NLGN1 (Kucukdereli et al., 2011; Lively and Brown, 2008b; Risher et al., 2014; Singh et al., 2016), it also binds NLGN2, which is found exclusively at inhibitory synapses. Hevin is expressed not only in glial cells but also by select inhibitory as well as excitatory neurons, so that hevin may strategically influence not only excitatory but also inhibitory synapse formation as well in select neural circuits (Mongrédien et al., 2019). Therefore, taken together, the impact of hevin on neurexin-neuroligin trans-synaptic bridges *in vivo* could be two-fold: 1) it could adhere neurexins and neuroligins together; and 2) it could counteract the inhibitory effect of MDGAs which are negative regulators of neurexin-neuroligin interaction. Thus, brain cells secreting hevin and SPARC may not only impact the overall number of synapses, but also the development of excitatory versus inhibitory synapses, independently, as a pair of proteins, as a trio through interplay with MDGAs, or an even larger network of proteins, thereby altering the excitation-inhibition balance in specific neural circuits and the overall communication through them. Targeted studies will be needed *ex vivo* and *in vivo* to dissect and resolve the importance of these different mechanisms in a synapse-specific, circuit-specific and brain region-specific way. ***Fifth***, while the SPARC FS domain interacts with β3-integrin (in particular residues TLEGTKKGHKLHLDYIGP), and SPARC secreted by astrocytes depresses the number of β3-integrin-stabilized AMPA-receptor subunits at synapses in an activity-dependent manner during development, hevin does not, even though it contains the nearly identical stretch of residues in a structurally similar conformation (**R**LEGTKKGH**Q**L**Q**LDY**F**G**A**) (Jones et al., 2011; Lane and Sage, 1990) (Figures 2 and 7G). Thus, despite the similarities between the hevin and SPARC FS domains, there are also important biological differences for which the molecular basis remains to be resolved. ***Sixth***, we show that hevin, like SPARC, binds collagen. This observation suggests that astrocytically secreted hevin and SPARC may couple neurexin-neuroligin trans-synaptic bridges to the extracellular matrix stabilizing them in the synaptic cleft. Taken together, our

data show that a portfolio of different synaptic proteins can impact neurexin-neuroligin trans-synaptic bridges by exploiting unique structure-function relationships, including overlapping binding sites and structurally conserved domains that compete.

Overall, our results suggest that the structure-function relationships of hevin and SPARC support both ***synergistic, antagonistic***, and ***independent*** roles in the brain. Our results also suggest that the neurexin-neuroligin trans-synaptic bridge is a focal point of control for synapse development, maturation, and maintenance, with a portfolio of different proteins (i.e., hevin, SPARC, and MDGAs) synergizing to either stabilize or destabilize these bridges (Figure 8). These insights may also be important from a therapeutic perspective, because alteration of hevin, through copy number variations (CNV), polymorphisms, mutations and altered protein levels, is linked to prevalent neuropsychiatric and neurodegenerative diseases, including depression, autism, schizophrenia, Alzheimer's, Parkinson's disease, multiple sclerosis (De Rubeis et al., 2014; Hammack et al., 2004; Jacquemont et al., 2006; Kähler et al., 2008; Purcell et al., 2001; Seddighi et al., 2018; Strunz et al., 2019; Yin et al., 2009; Zhurov et al., 2012). Likewise, mutations in neurexins and neuroligins are also implicated in many neuropsychiatric disorders, including autism spectrum disorder, schizophrenia, depression, and addiction, highlighting the importance of their trans-synaptic bridges for normal brain function (Südhof, 2008). Recently, hevin and SPARC were also identified as critical components of a chemoattractant complex, together with pleiotrophin and HSP90B; this complex is secreted by neural precursor cells in the lateral ventricle subventricular zone where it attracts glioma cells promoting their invasion, although the molecular mechanism of action is unclear (Qin et al., 2017). Underscoring its therapeutic relevance, hevin overexpression in the nucleus accumbens is sufficient to induce an antidepressant response in rodents suggesting a role in mediating endogenous resilience to stress (Vialou et al., 2010). Thus, it will be important to further delineate the exact molecular mechanisms by which both hevin and SPARC modulate protein interaction networks at the synapse and beyond in order to understand their roles in modulating neural circuits, their roles in the pathogenesis of specific neuropsychiatric and neurological disorders, and their therapeutic utility.

STAR Methods

RESOURCE AVAILABILITY

Lead Contact—Further information and requests for resources and reagents should be directed to and will be fulfilled by the Lead Contact, Gabby Rudenko (garudenk@utmb.edu).

Materials Availability—Unique/stable reagents generated in this study will be made available upon request as long as in stock; the University of Texas Medical Branch may require a completed Materials Transfer Agreement.

Data and Software Availability—The coordinates for hevin FS-EC have been deposited in the Protein Data Bank with accession number 7KBU.

EXPERIMENTAL MODEL AND SUBJECT DETAILS

Human hevin (accession number BC033721), human SPARC (accession number NM_003118) and their fragments followed by a C-terminal ASTSHHHHHH tag were produced using baculovirus-mediated overexpression in HighFive cells with Insect-XPRESS/L-Glutamine medium (Lonza) at 28°C for 72h. The following proteins were produced: human hevin_C1 (I^{17}-F^{664}), human hevin_C2 (V^{430}-F^{664}), hevin_C3 (Q^{365}-F^{664}), hevin_C4 (L^{302}-F^{664}), hevin_C5 (V^{430}-S^{511}), hevin_C6 (S^{511}-F^{664}); human SPARC_C1 (A^{18}–I^{303}), and SPARC_C2 (A^{68}-I^{303}).

METHOD DETAILS

Protein Expression and Purification—Briefly, medium containing the over-expressed and secreted proteins was concentrated after adding protease inhibitors (pepstatin, leupeptin and PMSF), dialyzed overnight (25 mM sodium phosphate, pH 8.0, 500mM NaCl), and purified on an Ni-NTA column (Invitrogen; equilibrated with 20 mM Tris-HCl, pH 7.9, 500 mM NaCl and eluted with an imidazole gradient) at 4°C. Subsequently, the protein was diluted (1:10) with 25 mM Tris-HCl, pH 8.0, applied to a Mono Q column (GE Healthcare; equilibrated with 25 mM Tris-HCl, pH 8.0, 50 mM NaCl) with contaminants binding to the column. Finally, the proteins were applied to a HiLoad Superdex-200 16/60 size exclusion column (GE Healthcare, equilibrated with 10 mM HEPES, pH 7.5, 50 mM NaCl). The purified proteins were concentrated and stored as flash-frozen aliquots at −80 °C. Yields were low for human hevin_C1, so this construct was not further pursued. We also generated the extracellular domains encoding rat NLGN2 (NM_053992; Val^{43}-His^{612}; with and without the splice insert SSA, amino acids GPLTKKRDEATLNPPDT) and NLGN2 mutants as described in the text; human NLGN1 (BC032555; D^{52}-N^{637}; without the SSA insert, with and without the SSB insert, amino acids GNRWSNSTK); bovine N1α L1L6 (NM_174404; M^{1}-S^{1339}; without splice inserts), n1α L1L5 (M^{1}-G^{1089}; without splice inserts), n1α L5L6 (A^{911}-S^{1339}; without splice inserts), n1α L2 (K^{258}-V^{475} which includes the splice insert SS1: EDNNVEGLAHLMMGDQGKSK), and n1α L2L3 (K^{258}-G^{675} which includes SS1); human MDGA1 Ig1-Ig2 (NM_153487; Y^{22}-T^{237}) and MDGA1 mutants as described in the text. NLGNs and mutants were purified as described in (Gangwar et al., 2017); the neurexins n1α L16, n1α L1L5, n1α L5L6 (Chen et al., 2011; Liu et al., 2018; Lu et al., 2014). MDGA1 and mutants were purified as described in (Gangwar et al., 2017); n1α L2 and n1α L2L3 were produced in *E. coli* as GST-fusion proteins and cleaved with thrombin as described in (Liu et al., 2018; Sheckler et al., 2006). Molecular weights and purity of all proteins were evaluated by SDS–PAGE and confirmed by mass spectrometry and N-terminal sequencing. Human collagen V isolated from placenta was purchased from Sigma/Aldrich (cat. nr. CC077).

Analytical Size Exclusion Chromatography (SEC)—Proteins hevin_C2 (120 μgr), hevin_C5 (80 μgr), hevin_C6 (60 μgr) and a mix of hevin_C5 + hevin_C6 (1:1 ratio, 140 μgr total) were applied in a 20 μl sample volume to a Superdex 200 Increase 3.2/300 column (equilibrated with running buffer: 20 mM HEPES, pH 7.5, 50 mM NaCl, 5 mM $CaCl_2$) at a flow rate of 0.02 ml/min. The column was calibrated with standards (Sigma) comprising cytochrome C (12,400 Da), carbonic anhydrase (29,000 Da), bovine serum albumin (66,000 Da), alcohol dehydrogenase (150,000 Da) and β-amylase (200,000 Da) dissolved in 10 mM

HEPES, pH 7.5, 50 mM NaCl, 0-20 mM $CaCl_2$ ensuring a matching running buffer. The elution profile of hevin_C2 (60 μgr) was also analyzed as a function of $CaCl_2$ in 10 mM HEPES, pH 7.5, 50 mM NaCl, 0-20 mM $CaCl_2$. All samples were run in duplicate.

Cross-linking studies—Hevin_C2 (60 μgr) was incubated with increasing amounts (0–10 mM) of disuccinimidyl sulfoxide (DSSO, Thermo Fisher) in 20 mM HEPES pH 8.0, 100 mM NaCl, 2 mM $CaCl_2$ at 20°C for 30 min at final concentration of 0.5 mg/ml. The cross-linking reaction was quenched by addition of 0.5 μl 1 M NH_4HCO_3 at 20°C for 15 minutes. As a positive control, NLGN2 which is a dimeric protein was cross-linked and analyzed as well. Samples were subsequently analyzed by SDS-PAGE under reducing conditions (+500 mM DTT).

Analytical Ultracentrifugation (AUC)—Sedimentation velocity (SV) experiments were performed to determine the oligomeric state of hevin_C2 using a Beckman Coulter Model XL-A analytical ultracentrifuge in 12 mm double sector (2-channel) cells with quartz windows and an An-60 Ti rotor at 42,000 rpm (141,995 RCF) at 20 °C. Prior to experiments, proteins were extensively dialyzed at 20 °C for 12 hours (in ~1000-fold volume of 10 mM HEPES pH 7.5, 50 mM NaCl, with or without 10 mM $CaCl_2$). This dialysis buffer was also used as the reference solution. Three different concentrations of hevin_C2 were analyzed (8 μM, 16 μM, and 25 μM) corresponding to OD_{280} values of 0.25, 0.5, and 0.8, respectively, in a sample volume of 400 μl. Absorbance scans of the cells were collected at 280 nm every 10 min with a step size of 0.003 cm. Hevin_C2 (25 mM, corresponding to OD_{280}=0.8) was also analyzed in 25 mM sodium acetate pH 4.5, 50 mM NaCl, 10 mM $CaCl_2$. Solvent density and viscosity, as well as estimates of the partial specific volume of hevin_C2 at 20 °C were calculated using SEDNTERP (Laue et al., 1992). Distribution and sedimentation coefficients of the sedimenting species were calculated from the SV data with SEDFIT version 14.81 (Schuck, 2000) using the continuous sedimentation coefficient distribution model $c(s)$. Standardization of S values ($s_{20,w}$) and generation of high-resolution plots were performed using Gussi 1.0.8 (Brautigam, 2015).

Crystallization and X-ray data collection—Crystals of hevin_C2 (FS-EC tandem) suitable for diffraction experiments were obtained via the hanging drop method at 20°C, by mixing 3 μl of protein solution (12 mg/ml in 10 mM Tris pH 7.5, 2 mM $CaCl_2$) with 3 μl of 22%(w/v) PEG 3350, 2.1 M sodium formate, 100 mM acetate pH 4.5, 100 mM $CaCl_2$, and equilibrating the drops against the latter solution as the reservoir solution. Diamond-shaped crystals with the symmetry of space group $I2_12_12_1$ grew in ~10 days up to 200 μm in length and diffracted to ~2.3 Å. Native crystals were cryo-protected in the reservoir solution supplemented with 15% (v/v) glycerol (final concentration) and flash-cooled in liquid nitrogen. A heavy-atom derivative was generated for phasing purposes; crystals were soaked in reservoir solution with 5 mM $HoCl_3$ (in order to replace Ca^{2+}-ions in the EC domain) for 2 h and then cryo-cooled as above. Data sets were collected at 100 K at the Advanced Photon Source (IMCA-CAT and LS-CAT) and processed with HKL2000 (Otwinowski and Minor, 1997); crystal cell dimensions and data statistics are given in Table 1.

Structure determination, experimental phasing and structural analysis—The hevin_C2 structure was determined by experimental phasing using the SIRAS (single isomorphous replacement with anomalous scattering) method with data collected from a native crystal ('Native 2') and a crystal derivatized with holmium (Table 1). Five heavy-atom sites were identified, and an initial model was built using the program AutoSol in PHENIX (Liebschner et al., 2019). Further model building was carried out iteratively with the program Coot (Emsley et al., 2010) interspersed with refinement using the Phenix program package. The resulting model was then refined against a higher-resolution, native dataset ('Native 1'). The refined model consists of two hevin molecules with molecule A (mol A) containing 221 residues (D^{431}-E^{544}, D^{557}-L^{663}) and molecule B (mol B) containing 194 residues (C^{438}-I^{443}, C^{454}-N^{542}, A^{568}-S^{666}). The electron density is poor in mol A for residues H^{545}-L^{556} between helices αA and αBC in the EC domain and in mol B for C^{444}-H^{453} in the Kazal subdomain and S^{543}-L^{567} between helices αA and αC in the EC domain. These residues were thus not incorporated in the model. The final model has good geometry (97.3 % in the favored region (404 residues), 2.7 % in the allowed region (11 residues) and no outliers in a Ramachandran plot) and includes two N-acetyl-glucosamines (NAG) attached to N^{476} in both hevin molecules, 2 calcium ions bound to the EF-hands of each hevin molecule, as well as two additional calcium ions (one bound between the two hevin molecules, and the other one bound to the EC domain of mol B), 4 formate molecules, 3 chloride ions, 1 sodium ion, and 155 water molecules.

Analysis of secondary structure elements was carried with the program STRIDE (Frishman and Argos, 1995); calculations of solvent-accessible and buried surfaces were performed with PDBe PISA (Krissinel and Henrick, 2007); protein interactions within 5 Å were assessed using the program NCONT; protein superpositions were carried out with the program gesamt (Krissinel, 2012) from the CCP4 package (CCP4, (Winn et al., 2011); and multi-sequence alignments were performed using Clustal Omega (Sievers et al., 2011) with figures generated using the ESPript 3.0 server (Robert and Gouet, 2014). Sequence homology comparisons were carried out with the following sequences: hevin (human, Q14515; bovine, Q3SYW7; naked mole rat, XP_004870609.1; mouse, P70663; dog, E2RPF3; and chinchilla, XP_005401392.1); SPARC (human, CAG33080.1; bovine, NP_776889.1; naked mole rat, EHB10683.1; mouse, CAJ18514.1; dog, CAJ18514.1; and chinchilla, XP_005376224.1); NLGN1 (human, ADB12633.1; bovine, NP_001192902.1; rat, NP_446320.1; mouse, NP_619607.2); NLGN2 (human, AAM46111.1; bovine, NP_001178171.1; rat, AAA97870.1; mouse, EDL12455.1); NLGN3 (human, ADB12634.1; bovine, AAI23786.1; rat, AAA97871.1; mouse, AAI50774.1). Residue conservation is as defined in Clustal-Omega (Sievers et al., 2011), i.e., an asterisk (*) signifies positions with a single, fully conserved residue; a colon (:) the equivalencies STA, NEQK, NHQK, NDEQ, QHRK, MILV, MILF, HY, FYW; and a period (.) the equivalencies CSA, ATV, SAG, STNK, STPA, SGND, SNDEQK, NDEQHK, NEQHRK, FVLIM, HFY. Structural representations were generated using the PyMol Molecular Graphics System, Schrödinger, LLC.

Surface Plasmon Resonance—Binding of hevin and SPARC proteins to NLGN2(+A) was assessed in Running Buffer (20 mM HEPES pH 7.5, 50 mM NaCl, 2 mM $CaCl_2$, 0.005% Tween 20) at 25 °C with a Biacore T100 system. NLGN2(+A) was immobilized on

two different C1 sensor chips (GE Healthcare) with 1273 and 1458 RU, respectively, in order to carry out two independent experiments. Specific binding data were obtained by injecting a series of hevin concentrations over an NLGN2(+A)-coupled sensor and subtracting the signal that was obtained by flowing the same series simultaneously over a sensor with no ligand immobilized. For each hevin construct (hevin_C2 through hevin_C6) the following concentrations were used: (0, 250, 500, 1000, 2000, and 4000 nM) and for each SPARC construct (SPARC_C1 and SPARC_C2) the following concentrations were used: (0, 31.25, 62.5, 125, 250, 500, 1000, 2000, and 4000 nM). The samples flowed on the chip at 30 μl/min for 120 s (association step) followed by Running Buffer only for 120 s (dissociation step). N1α_L1L6 (0, 1.875, 3.75, 7.5, 15, and 30 nM) was used as a positive control for binding to NLGN2(+A), and N1α_L2 (0, 3.125, 6.25, 12.5, 25, and 50 nM) was used as a negative control. The sensor was regenerated after each protein injection with 1 x HEPES Buffered Saline (HBS), 1000 mM NaCl, 3 mM EDTA. Data were processed using a kinetic analysis, and K_D values were calculated from sensorgram data fit to a 1:1 stoichiometric model. Data were fit using a R_{max} local fitting method. K_D values for a given construct were derived by averaging the values obtained from two independent experiments with two separately immobilized sensor chips (averages and standard deviations) are given.

Binding of Hevin_C6 to human collagen V was assessed by SPR in Running Buffer (10 mM HEPES pH 7.4, 150 mM NaCl, 2 mM $CaCl_2$, 0.05% (v/v) Surfactant P20 at 25 °C. Collagen V was immobilized on two different CM5 sensor chips (GE Healthcare) with 4262 and 4889 RU, respectively, in order to carry out two independent experiments. Specific binding data were obtained by injecting a series of hevin_C6 concentrations over a collagen V-coupled sensor and subtracting the signal that was obtained by flowing the same series simultaneously over a sensor with no ligand immobilized. The following concentrations were used: (0, 1, 2, 4, 8, 16 μM). The samples flowed on the chip at 30 μl/min for 60 s (association step) followed by Running Buffer only for 120 s (dissociation step). The sensor was regenerated after each protein injection with 3 mM NaOH. Data were processed as above.

Protein Labeling—Hevin and SPARC proteins were labeled using the OneQuant (5/6)-TAMRA-SE fluorescent probe (G-Biosciences). We first dissolved the fluorescent probe in 100% DMSO and then added the protein sample in 10 mM HEPES pH 7.5, 50 mM NaCl with final concentrations of 100 μM (protein) and 1000 μM (probe), respectively. The reaction mixture was incubated at room temperature for 2 hr in the dark. The labeled proteins were purified using SpinOUT GT-600 columns (G-Biosciences). The concentration of each TAMRA-labelled protein was determined using UV absorption at 247 nm. Finally, the labeling efficiency for each protein was determined to ensure that more than 1 TAMRA molecule was attached per molecule of protein. All experiments involving labeled proteins in this study were done while minimizing their exposure time to light.

Fluorescence Polarization—A fluorescence polarization (FP) assay was used to measure the binding affinity between different TAMRA-labeled proteins and their potential partners, i.e., neuroligins, neurexin 1α, MDGA1, as well as mutants and fragments of these proteins. Assays were performed in 96-well black flat-bottom plates (Corning-3991) using a

PHERAstar microplate reader (BMG Labtech) with excitation at 540 nm and emission at 590 nm using 200 flashes per well at 25 °C.

For binding to neuroligins, a concentration series of 0-300 nM NLGNs were prepared by serial dilution and mixed with a final concentration of 30 nM TMR-labeled hevin_C2, hevin_C5 or hevin_C6 in FP buffer (10 mM HEPES pH 7.5, 25 mM NaCl, 0.005% (v/v) Triton X100) in a final volume of 100 μl/well. The plates were incubated for 10-20 min with gentle shaking and protecting from light before measuring the fluorescence values. Mutants of NLGN2(+A) (described first in (Gangwar et al., 2017) were also tested for their binding to TMR-hevin_C5 with a concentration series of 0-150 nM NLGN2(+A) mutant prepared by serial dilution and mixed with an end concentration of 30 nM TMR-labeled hevin_C5 in FP buffer in a final volume of 100 μl/well. In parallel, a concentration series of 0-300 nM NLGN2(+A) was prepared by serial dilution and mixed with an end concentration of 30 nM TMR-labeled SPARC_C1 or SPARC_C2 in FP buffer in a final volume of 100 μl/well, and then the plates were incubated 10-20 min as described above. Before reading fluorescence values, the target value was set to 50 mP for the TMR-labeled tracer by adjusting the gain on a well with 30 nM TAMRA in H_2O. For most experiments, the 0 nM unlabeled partner concentration was set as the baseline value and subtracted from all the values measured. All experiments were carried out in triplicates. Data were processed using Prism 6.0 (GraphPad Software), fitting the binding curves to a ‘One Site-Total Binding’ model. Each data point represents the mean of the triplicates, and the error bar represents the standard deviation. K_D values and their standard deviation were calculated by averaging two independent sets of experiments together.

To assess the direct binding of hevin_C5 to MDGA1_C8 and MDGA1_C8_Mut4 using a FP assay, TMR-labeled hevin_C5 was incubated with a concentration series of 0-300 nM MDGA1_C8 and MDGA1_C8_Mut4 in 10 mM HEPES pH 7.5, 100 mM NaCl, 0.005% (v/v) Triton X-100. For comparison, NLGN2(+A) was taken along as a positive control for binding to TMR-labeled hevin_C5. The plates were incubated 10-20 min as described above. All experiments were carried out in triplicates. Data were collected and processed as described above.

For binding to neurexins, concentration series of 0-50 nM n1α L1L6, n1α L5L6, n1α L1L5, or n1α L2L3, were prepared by serial dilution and mixed with an end concentration of 20 nM TMR-labeled hevin_C5 in FP buffer with 2 mM $CaCl_2$ (for Ca^{2+}-containing conditions) or 10 mM EGTA (for Ca^{2+}-free conditions), in a final volume of 100 μl/well. To assess the binding of SPARC to neurexin, SPARC_C1 was incubated with the same panel of neurexins as described above (0-100 nM) in FP buffer with 2 mM $CaCl_2$ or 10 mM EGTA, respectively. The plates were incubated 10-20 min as described above. All experiments were carried out in triplicates. Data were collected and processed as described above.

To assess the binding of the hevin EC to human collagen V, TMR-labeled hevin_C6 was incubated with a concentration series of 0-50 nM collagen V in 10 mM HEPES pH 7.4, 50 mM NaCl, 0.005% (v/v) Triton X-100 in presence of 2 mM $CaCl_2$ (Ca^{2+}-containing conditions) or 10 mM EGTA (Ca^{2+}-free conditions). For comparison, the hevin FS domain

(TMR-labeled hevin_C5) was also assessed for its binding to collagen V using the same buffer. Data were collected and processed as described above.

Competitive Binding Assay—To measure the ability of unlabeled hevin_C2, SPARC_C1, and SPARC_C2 to disrupt the complex between the hevin FS domain (hevin_C5) and NLGN2(+A), a modified FP assay was used. First, the hevin_C5:NLGN2(+A) complex was prepared by mixing 5 nM TMR-hevin_C5 and 100 nM NLGN2(+A) in FP buffer. Subsequently, the complex was combined with a serial dilution of either unlabeled hevin_C2, SPARC_C1 or SPARC_C2 (0-4000 nM) and dispensed in 96-well flat-bottom black assay plates (Corning-3991) in a final volume of 100 μl/well. To measure the ability of MDGA1_C8 (which contains MDGA1 Ig1-Ig2), and MDGA1_C8 Mut4 (which contains MDGA1 Ig1-Ig2 $R^{105}A$, $Y^{107}A$, $R^{123}A$, $F^{154}A$, $R^{156}A$, $Y^{187}A$ and exhibits weakened affinity for NLGN2 (Gangwar et al., 2017) to disrupt the complex between hevin_C5:NLGN2(+A), we also used a modified FP assay. First, the hevin_C5:NLGN2(+A) complex was prepared by mixing 5 nM TMR-hevin_C5 and 100 nM NLGN2(+A) in FP buffer. Subsequently, the complex was combined with a serial dilution of either unlabeled MDGA1_C8 or MDGA1_C8 Mut4 (0-4000 nM) and dispensed in 96-well flat-bottom black assay plates (Corning-3991) so that each well received a final volume of 100 μl complex. Plates were incubated at room temperature for 1 hr with gentle shaking and the FP signal measured using the Pherastar plate reader at 25 °C (excitation at 540 nm, emission at 590 nm, 200 flashes per well). Before reading a plate, the target value was set to 50 mP by adjusting the gain on a well with 5 nM TAMRA in H_2O. Data were processed as above. Each data point represents the mean of triplicates, and the error bar represents the standard deviation.

Tripartite binding assay—To assess whether TAMRA-labeled hevin_C5 (TMR-hevin_C5), NLGNs and n1α form a tripartite protein complex, we used an optimized FP assay. First, the TMR-hevin_C5:n1α L5L6 or TMR-hevin_C5:n1α L2L3 complex (as a control for poor binding) was prepared by mixing 5 nM TMR-hevin_C5 and 50 nM n1α L5L6 or n1α L2L3 in FP buffer with 2 mM $CaCl_2$, followed by incubation for 10 −15 min at room temperature. Subsequently, the complex was mixed with a serial dilution of either unlabeled NLGN1(−A,+B) or NLGN2(+A) (0 – 300 nM) in 96-well flat-bottom black assay plates (Corning-3991) in a final volume of 100 μl complex per well (final concentrations: 5 nM TMR-hevin_C5, 50 nM n1α L5L6 or n1α L2L3, with the serial dilution of NLGN1(−A,+B) or NLGN2(+A)). Plates were incubated at room temperature for 30 min with gentle shaking and the FP signal measured using a Pherastar plate reader at 25 °C (excitation at 540 nm, emission at 590 nm, 200 flashes per well). The target value was set to 50 mP for TAMRA as before. Data were processed as above. Each data point represents the mean of triplicates, and the error bar represents the standard deviation.

Quantification and Statistical Analysis—The crystal structure of Hevin FS-EC was determined using materials and software listed in the Key Resources Table. Statistics from the X-ray crystallographic data processing, phasing, refinement, and structure validation software packages are displayed in Table 1. Fluorescence polarization data were processed using Prism 6.0 (GraphPad Software). For fluorescence polarization experiments, K_D values

indicated in Figures 3B, 3D and 5B are shown as mean ± standard deviation (described in the Method Details and indicated in the legends), while for Figures 4B, 4C, 4D, 5D, 5E, 6B, 6C, and 7E, binding was assessed qualitatively (as described in the Method Details). All SPR data were analyzed with the Biacore T100 evaluation software using a kinetic analysis, and K_D values were calculated from sensorgram data fit to a 1:1 stoichiometric model. Data were fit using a R_{max} local fitting method. K_D values in Figure 3C and 5C (shown as mean ± standard deviation) were derived by averaging the values obtained from two independent experiments, while Figure 7F was assessed qualitatively (as described in the Method Details and indicated in the legends). SV-AUC experiments were performed in duplicates (one set of representative results are shown in Figure S2C). The experimental data was analyzed using the software SEDNTERP, SEDFIT and Gussi 1.0 as described in the Method Details. Analytical size exclusion chromatography (SEC) experiments shown in Figures 1E and S2D were performed in two independent experiments; the average elution volumes (EVs) with standard deviation are shown in Figure 1E with appropriate calibration markers run in parallel in order to calculate the apparent molecular weights, MW_{exp} (as described in the Method Details and indicated in the legends).

Supplementary Material

Refer to Web version on PubMed Central for supplementary material.

Acknowledgements:

This work was funded by NIMH (R01MH077303), and the SCSB at UTMB. The Advanced Photon Source (IMCA-CAT, LS-CAT, and SBC-CAT) and the Advanced Light Source are thanked for access to synchrotron radiation.

References

Albrecht D, López-Murcia FJ, Pérez-González AP, Lichtner G, Solsona C, and Llobet A (2012). SPARC prevents maturation of cholinergic presynaptic terminals. Mol. Cell. Neurosci 49, 364–374. [PubMed: 22306863]

Allen NJ, and Eroglu C (2017). Cell Biology of Astrocyte-Synapse Interactions. Neuron 96, 697–708. [PubMed: 29096081]

Bemben MA, Shipman SL, Nicoll RA, and Roche KW (2015). The cellular and molecular landscape of neuroligins. Trends Neurosci. 38, 496–505. [PubMed: 26209464]

Bradshaw AD (2009). The role of SPARC in extracellular matrix assembly. Journal of Cell Communication and Signaling 3, 239–246. [PubMed: 19798598]

Bradshaw AD (2012). Diverse biological functions of the SPARC family of proteins. Int. J. Biochem. Cell Biol 44, 480–488. [PubMed: 22249026]

Brautigam CA (2015). Chapter Five - Calculations and Publication-Quality Illustrations for Analytical Ultracentrifugation Data. In Methods in Enzymology, Cole JL, ed. (Academic Press), pp. 109–133.

Chen F, Venugopal V, Murray B, and Rudenko G (2011). The structure of neurexin 1α reveals features promoting a role as synaptic organizer. Structure 19, 779–789. [PubMed: 21620716]

Connor SA, Ammendrup-Johnsen I, Chan AW, Kishimoto Y, Murayama C, Kurihara N, Tada A, Ge Y, Lu H, Yan R, et al. (2016). Altered Cortical Dynamics and Cognitive Function upon Haploinsufficiency of the Autism-Linked Excitatory Synaptic Suppressor MDGA2. Neuron 91, 1052–1068. [PubMed: 27608760]

Connor SA, Elegheert J, Xie Y, and Craig AM (2019). Pumping the brakes: suppression of synapse development by MDGA-neuroligin interactions. Curr. Opin. Neurobiol 57, 71–80. [PubMed: 30771697]

De Rubeis S, He X, Goldberg AP, Poultney CS, Samocha K, Cicek AE, Kou Y, Liu L, Fromer M, Walker S, et al. (2014). Synaptic, transcriptional and chromatin genes disrupted in autism. Nature 515, 209–215. [PubMed: 25363760]

Elegheert J, Cvetkovska V, Clayton AJ, Heroven C, Vennekens KM, Smukowski SN, Regan MC, Jia W, Smith AC, Furukawa H, et al. (2017). Structural Mechanism for Modulation of Synaptic Neuroligin-Neurexin Signaling by MDGA Proteins. Neuron 95, 896–913.e10. [PubMed: 28817804]

Emsley P, Lohkamp B, Scott WG, and Cowtan K (2010). Features and development of Coot. Acta Crystallogr. D Biol. Crystallogr 66, 486–501. [PubMed: 20383002]

Ferrer-Ferrer M, and Dityatev A (2018). Shaping Synapses by the Neural Extracellular Matrix. Frontiers in Neuroanatomy 12, 40. [PubMed: 29867379]

Frishman D, and Argos P (1995). Knowledge-based protein secondary structure assignment. Proteins 23, 566–579. [PubMed: 8749853]

Gan KJ, and Südhof TC (2019). Specific factors in blood from young but not old mice directly promote synapse formation and NMDA-receptor recruitment. Proc Natl Acad Sci U S A 116, 12524–12533. [PubMed: 31160442]

Gan KJ, and Südhof TC (2020). SPARCL1 Promotes Excitatory But Not Inhibitory Synapse Formation and Function Independent of Neurexins and Neuroligins. J Neurosci 40, 8088–8102. [PubMed: 32973045]

Gangwar SP, Zhong X, Seshadrinathan S, Chen H, Machius M, and Rudenko G (2017). Molecular Mechanism of MDGA1: Regulation of Neuroligin 2:Neurexin Trans-synaptic Bridges. Neuron 94, 1132–1141.e4. [PubMed: 28641112]

Girard JP, and Springer TA (1995). Cloning from purified high endothelial venule cells of hevin, a close relative of the antiadhesive extracellular matrix protein SPARC. Immunity 2, 113–123. [PubMed: 7600298]

Giudici C, Raynal N, Wiedemann H, Cabral WA, Marini JC, Timpl R, Bächinger HP, Farndale RW, Sasaki T, and Tenni R (2008). Mapping of SPARC/BM-40/osteonectin-binding sites on fibrillar collagens. J. Biol. Chem 283, 19551–19560. [PubMed: 18487610]

Hambrock HO, Nitsche DP, Hansen U, Bruckner P, Paulsson M, Maurer P, and Hartmann U (2003). SC1/hevin. An extracellular calcium-modulated protein that binds collagen I. J. Biol. Chem 278, 11351–11358. [PubMed: 12538579]

Hammack BN, Fung KYC, Hunsucker SW, Duncan MW, Burgoon MP, Owens GP, and Gilden DH (2004). Proteomic analysis of multiple sclerosis cerebrospinal fluid. Mult. Scler 10, 245–260. [PubMed: 15222687]

Hashimoto N, Sato T, Yajima T, Fujita M, Sato A, Shimizu Y, Shimada Y, Shoji N, Sasano T, and Ichikawa H (2016). SPARCL1-containing neurons in the human brainstem and sensory ganglion. Somatosens Mot Res 33, 112–117. [PubMed: 27357901]

Hohenester E, Maurer P, Hohenadl C, Timpl R, Jansonius JN, and Engel J (1996). Structure of a novel extracellular Ca(2+)-binding module in BM-40. Nat. Struct. Biol 3, 67–73. [PubMed: 8548457]

Hohenester E, Maurer P, Timpl R (1997). Crystal structure of a pair of follistatin-like and EF-hand calcium-binding domains in BM-40. EMBO J. 16, 3778–3786. [PubMed: 9233787]

Hohenester E, Sasaki T, Giudici C, Farndale RW, and Bächinger HP (2008). Structural basis of sequence-specific collagen recognition by SPARC. Proc. Natl. Acad. Sci. U.S.A 105, 18273–18277. [PubMed: 19011090]

Jacquemont M-L, Sanlaville D, Redon R, Raoul O, Cormier-Daire V, Lyonnet S, Amiel J, Le Merrer M, Heron D, de Blois M-C, et al. (2006). Array-based comparative genomic hybridisation identifies high frequency of cryptic chromosomal rearrangements in patients with syndromic autism spectrum disorders. J. Med. Genet 43, 843–849. [PubMed: 16840569]

Jones EV, and Bouvier DS (2014). Astrocyte-secreted matricellular proteins in CNS remodelling during development and disease. Neural Plast. 2014, 321209. [PubMed: 24551460]

Jones EV, Bernardinelli Y, Tse YC, Chierzi S, Wong TP, and Murai KK (2011). Astrocytes control glutamate receptor levels at developing synapses through SPARC-beta-integrin interactions. J. Neurosci 31, 4154–4165. [PubMed: 21411656]

Kähler AK, Djurovic S, Kulle B, Jönsson EG, Agartz I, Hall H, Opjordsmoen S, Jakobsen KD, Hansen T, Melle I, et al. (2008). Association analysis of schizophrenia on 18 genes involved in neuronal migration: MDGA1 as a new susceptibility gene. Am. J. Med. Genet. B Neuropsychiatr. Genet 147B, 1089–1100. [PubMed: 18384059]

Kim JA, Kim D, Won SY, Han KA, Park D, Cho E, Yun N, An HJ, Um JW, Kim E, et al. (2017). Structural Insights into Modulation of Neurexin-Neuroligin Trans-synaptic Adhesion by MDGA1/Neuroligin-2 Complex. Neuron 94, 1121–1131.e6. [PubMed: 28641111]

Krissinel E (2012). Enhanced fold recognition using efficient short fragment clustering. J Mol Biochem 1, 76–85. [PubMed: 27882309]

Krissinel E, and Henrick K (2007). Inference of macromolecular assemblies from crystalline state. J. Mol. Biol 372, 774–797. [PubMed: 17681537]

Kucukdereli H, Allen NJ, Lee AT, Feng A, Ozlu MI, Conatser LM, Chakraborty C, Workman G, Weaver M, Sage EH, et al. (2011). Control of excitatory CNS synaptogenesis by astrocyte-secreted proteins Hevin and SPARC. Proc. Natl. Acad. Sci. U.S.A 108, E440–449. [PubMed: 21788491]

Lane TF, and Sage EH (1990). Functional mapping of SPARC: peptides from two distinct Ca+(+)-binding sites modulate cell shape. J. Cell Biol 111, 3065–3076. [PubMed: 2269665]

Laue TM, Shah BD, Ridgeway TM, and Pelletier SL (1992). Analyticall Ultracentrifugation in Biochemistry and Polymer Science. Harding S, and Rowe A, eds. (Royal Society of Chemistry), pp. 90–125.

Lee K, Kim Y, Lee S-J, Qiang Y, Lee D, Lee HW, Kim H, Je HS, Südhof TC, and Ko J (2013). MDGAs interact selectively with neuroligin-2 but not other neuroligins to regulate inhibitory synapse development. Proc. Natl. Acad. Sci. U.S.A 110, 336–341. [PubMed: 23248271]

Lein ES, Hawrylycz MJ, Ao N, Ayres M, Bensinger A, Bernard A, Boe AF, Boguski MS, Brockway KS, Byrnes EJ, et al. (2007). Genome-wide atlas of gene expression in the adult mouse brain. Nature 445, 168–176. [PubMed: 17151600]

Liebschner D, Afonine PV, Baker ML, Bunkóczi G, Chen VB, Croll TI, Hintze B, Hung LW, Jain S, McCoy AJ, et al. (2019). Macromolecular structure determination using X-rays, neutrons and electrons: recent developments in Phenix. Acta Crystallogr D Struct Biol 75, 861–877. [PubMed: 31588918]

Liu J, Misra A, Reddy MVVVS, White MA, Ren G, and Rudenko G (2018). Structural Plasticity of Neurexin 1α: Implications for its Role as Synaptic Organizer. J. Mol. Biol 430, 4325–4343. [PubMed: 30193986]

Lively S, and Brown IR (2008a). Localization of the extracellular matrix protein SC1 coincides with synaptogenesis during rat postnatal development. Neurochem. Res. 33, 1692–1700. [PubMed: 18335312]

Lively S, and Brown IR (2008b). The extracellular matrix protein SC1/hevin localizes to excitatory synapses following status epilepticus in the rat lithium-pilocarpine seizure model. J. Neurosci. Res. 86, 2895–2905. [PubMed: 18488994]

Lively S, Ringuette MJ, and Brown IR (2007). Localization of the extracellular matrix protein SC1 to synapses in the adult rat brain. Neurochem. Res 32, 65–71. [PubMed: 17151913]

Lloyd-Burton S, and Roskams AJ (2012). SPARC-like 1 (SC1) is a diversely expressed and developmentally regulated matricellular protein that does not compensate for the absence of SPARC in the CNS. J. Comp. Neurol 520, 2575–2590. [PubMed: 22173850]

López-Murcia FJ, Terni B, and Llobet A (2015). SPARC triggers a cell-autonomous program of synapse elimination. Proc. Natl. Acad. Sci. U.S.A 112, 13366–13371. [PubMed: 26420865]

Lu Z, Wang Y, Chen F, Tong H, Reddy MS, Luo L, Seshadrinathan S, Zhang L, Holthauzen LMF, and Craig AM (2014). Calsyntenin-3 molecular architecture and interaction with neurexin 1α. Journal of Biological Chemistry 289, 34530–34542.

Maurer P, Göhring W, Sasaki T, Mann K, Timpl R, and Nischt R (1997). Recombinant and tissue-derived mouse BM-40 bind to several collagen types and have increased affinities after proteolytic activation. Cell. Mol. Life Sci 53, 478–484. [PubMed: 9176569]

Mendis DB, Malaval L, and Brown IR (1995). SPARC, an extracellular matrix glycoprotein containing the follistatin module, is expressed by astrocytes in synaptic enriched regions of the adult brain. Brain Res. 676, 69–79. [PubMed: 7796180]

Mendis DB, Shahin S, Gurd JW, and Brown IR (1996). SC1, a SPARC-related glycoprotein, exhibits features of an ECM component in the developing and adult brain. Brain Res. 713, 53–63. [PubMed: 8724975]

Mongrédien R, Erdozain AM, Dumas S, Cutando L, Del Moral AN, Puighermanal E, Rezai Amin S, Giros B, Valjent E, Meana JJ, et al. (2019). Cartography of hevin-expressing cells in the adult brain reveals prominent expression in astrocytes and parvalbumin neurons. Brain Struct Funct 224, 1219–1244. [PubMed: 30656447]

Murphy-Ullrich JE, and Sage EH (2014). Revisiting the matricellular concept. Matrix Biol. 37, 1–14. [PubMed: 25064829]

Otwinowski Z, and Minor W (1997). Processing of X-ray diffraction data collected in oscillation mode. Macromol Crystallogr A 276: 307–326.

Pettem KL, Yokomaku D, Takahashi H, Ge Y, and Craig AM (2013). Interaction between autism-linked MDGAs and neuroligins suppresses inhibitory synapse development. J Cell Biol jcb–201206028.

Purcell AE, Jeon OH, Zimmerman AW, Blue ME, and Pevsner J (2001). Postmortem brain abnormalities of the glutamate neurotransmitter system in autism. Neurology 57, 1618–1628. [PubMed: 11706102]

Qin EY, Cooper DD, Abbott KL, Lennon J, Nagaraja S, Mackay A, Jones C, Vogel H, Jackson PK, and Monje M (2017). Neural Precursor-Derived Pleiotrophin Mediates Subventricular Zone Invasion by Glioma. Cell 170, 845–859.e19. [PubMed: 28823557]

Risher WC, Patel S, Kim IH, Uezu A, Bhagat S, Wilton DK, Pilaz L-J, Singh Alvarado J, Calhan OY, Silver DL, et al. (2014). Astrocytes refine cortical connectivity at dendritic spines. Elife 3.

Robert X, and Gouet P (2014). Deciphering key features in protein structures with the new ENDscript server. Nucleic Acids Res. 42, W320–324. [PubMed: 24753421]

Rudenko G (2019). Neurexins - versatile molecular platforms in the synaptic cleft. Curr. Opin. Struct. Biol 54, 112–121. [PubMed: 30831539]

Rudenko G, Nguyen T, Chelliah Y, Sudhof TC, and Deisenhofer J (1999). The structure of the ligand-binding domain of neurexin Ib: regulation of LNS domain function by alternative splicing. Cell 99, 93–102. [PubMed: 10520997]

Sasaki T, Hohenester E, Gohring W, Timpl R (1998). Crystal structure and mapping by site-directed mutagenesis of the collagen-binding epitope of an activated form of BM-40/SPARC/osteonectin. EMBO J. 17, 1625–1634. [PubMed: 9501084]

Schuck P (2000). Size-distribution analysis of macromolecules by sedimentation velocity ultracentrifugation and lamm equation modeling. Biophys. J 78, 1606–1619. [PubMed: 10692345]

Seddighi S, Varma VR, An Y, Varma S, Beason-Held LL, Tanaka T, Kitner-Triolo MH, Kraut MA, Davatzikos C, and Thambisetty M (2018). SPARCL1 Accelerates Symptom Onset in Alzheimer's Disease and Influences Brain Structure and Function During Aging. J. Alzheimers Dis 61, 401–414. [PubMed: 29154276]

Sheckler LR, Henry L, Sugita S, Südhof TC, and Rudenko G (2006). Crystal Structure of the Second LNS/LG Domain from Neurexin 1α Ca2+ BINDING AND THE EFFECTS OF ALTERNATIVE SPLICING. Journal of Biological Chemistry 281, 22896–22905.

Sievers F, Wilm A, Dineen D, Gibson TJ, Karplus K, Li W, Lopez R, McWilliam H, Remmert M, Söding J, et al. (2011). Fast, scalable generation of high-quality protein multiple sequence alignments using Clustal Omega. Mol. Syst. Biol 7, 539. [PubMed: 21988835]

Singh SK, Stogsdill JA, Pulimood NS, Dingsdale H, Kim YH, Pilaz L-J, Kim IH, Manhaes AC, Rodrigues WS, Pamukcu A, et al. (2016). Astrocytes Assemble Thalamocortical Synapses by Bridging NRX1α and NL1 via Hevin. Cell 164, 183–196. [PubMed: 26771491]

Strunz M, Jarrell JT, Cohen DS, Rosin ER, Vanderburg CR, and Huang X (2019). Modulation of SPARC/Hevin Proteins in Alzheimer's Disease Brain Injury. J. Alzheimers Dis 68, 695–710. [PubMed: 30883351]

Südhof TC (2008). Neuroligins and neurexins link synaptic function to cognitive disease. Nature 455, 903–911. [PubMed: 18923512]

Südhof TC (2017). Synaptic Neurexin Complexes: A Molecular Code for the Logic of Neural Circuits. Cell 171, 745–769. [PubMed: 29100073]

Sullivan MM, Barker TH, Funk SE, Karchin A, Seo NS, Höök M, Sanders J, Starcher B, Wight TN, Puolakkainen P, et al. (2006). Matricellular hevin regulates decorin production and collagen assembly. J. Biol. Chem 281, 27621–27632. [PubMed: 16844696]

Vialou V, Robison AJ, Laplant QC, Covington HE, Dietz DM, Ohnishi YN, Mouzon E, Rush AJ, Watts EL, Wallace DL, et al. (2010). DeltaFosB in brain reward circuits mediates resilience to stress and antidepressant responses. Nat. Neurosci 13, 745–752. PMC2895556. [PubMed: 20473292]

Vincent AJ, Lau PW, and Roskams AJ (2008). SPARC is expressed by macroglia and microglia in the developing and mature nervous system. Dev. Dyn 237, 1449–1462. [PubMed: 18366138]

Winn MD, Ballard CC, Cowtan KD, Dodson EJ, Emsley P, Evans PR, Keegan RM, Krissinel EB, Leslie AG, and McCoy A (2011). Overview of the CCP4 suite and current developments. Acta Crystallographica Section D: Biological Crystallography 67, 235–242. [PubMed: 21460441]

Yin GN, Lee HW, Cho J-Y, and Suk K (2009). Neuronal pentraxin receptor in cerebrospinal fluid as a potential biomarker for neurodegenerative diseases. Brain Res. 1265, 158–170. [PubMed: 19368810]

Yuzaki M (2018). Two Classes of Secreted Synaptic Organizers in the Central Nervous System. Annu. Rev. Physiol 80, 243–262. [PubMed: 29166241]

Zhurov V, Stead JDH, Merali Z, Palkovits M, Faludi G, Schild-Poulter C, Anisman H, and Poulter MO (2012). Molecular pathway reconstruction and analysis of disturbed gene expression in depressed individuals who died by suicide. PLoS ONE 7, e47581. [PubMed: 23110080]

Highlights

- An elaborate protein network regulates neurexin-neuroligin trans-synaptic bridges.
- The hevin FS domain binds both neurexin and neuroligin via a direct interaction.
- Antagonist SPARC also binds neurexin/neuroligin.
- Hevin and MDGAs, which exert opposite action, compete for binding to neuroligin.

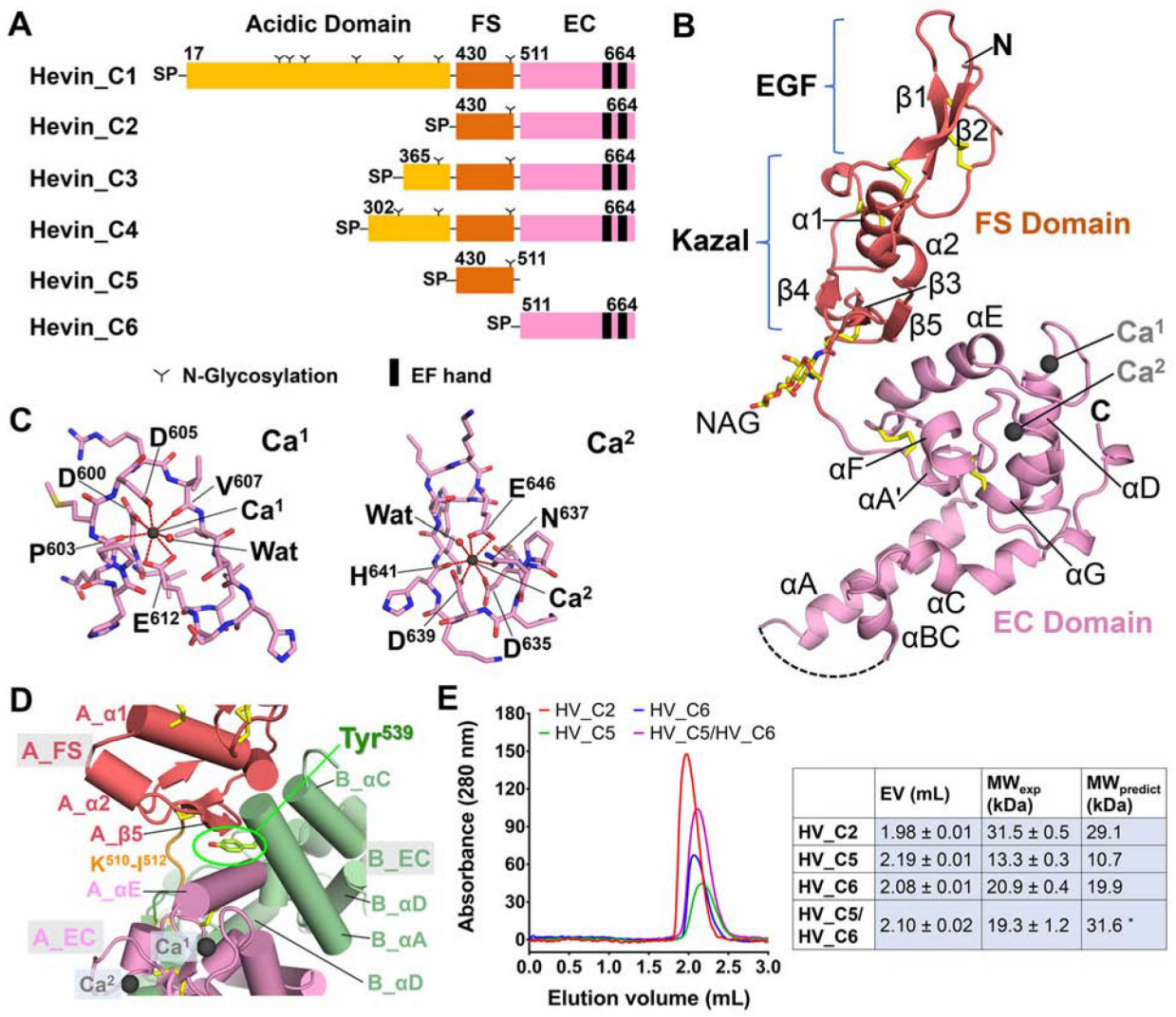

	EV (mL)	MW_{exp} (kDa)	$MW_{predict}$ (kDa)
HV_C2	1.98 ± 0.01	31.5 ± 0.5	29.1
HV_C5	2.19 ± 0.01	13.3 ± 0.3	10.7
HV_C6	2.08 ± 0.01	20.9 ± 0.4	19.9
HV_C5/ HV_C6	2.10 ± 0.02	19.3 ± 1.2	31.6 *

Figure 1. 3D structure of hevin FS-EC.

(A) Domain structure of hevin constructs used in this study. SP, signal peptide; FS, follistatin-like domain; EC, extracellular calcium binding domain.

(B) Hevin FS-EC structure. Disulfide bonds are shown as yellow sticks, calcium ions as dark grey balls, and glycan moieties (NAG-NAG) in stick representation. The N- and C- termini are indicated. Dashes indicate a disordered region.

(C) Ca^{2+}-binding sites in the EF hands (EF1, left and EF2, right) reveal pentagonal bipyramidal coordination spheres. Ca^{2+} ions are shown as dark gray spheres and Ca^{2+}-coordinating residues are labeled. The Ca^{2+}-binding site in EF1 is composed of D^{600}, D^{605} and E^{612}, P^{603}, V^{607}, and a water molecule. The Ca^{2+}-binding site in EF2 is composed of D^{635}, N^{637}, D^{639}, E^{646}, H^{641}, and a water molecule.

(D) The interface between the FS (coral) and EC (pink) domains in mol A is stabilized by insertion of the EC domain (pale green) of mol B, in particular Tyr^{539}.

(E) Analysis of hevin domains (HV_C2 through HV_C6) by analytical size exclusion chromatography (SEC). Samples were run in duplicate, and the average elution volume (EVs) with standard deviation is listed. Calibration standards, also run in duplo, deviated

<0.02 ml between runs. Apparent molecular weights (MW_{exp}) estimated from the elution volumes assuming a globular shape, and the predicted molecular weights based on amino acid composition ($MW_{predict}$) are shown. *, sum of the predicted molecular weights for the isolated FS and EC domains.

See also Figures S1 and S2.

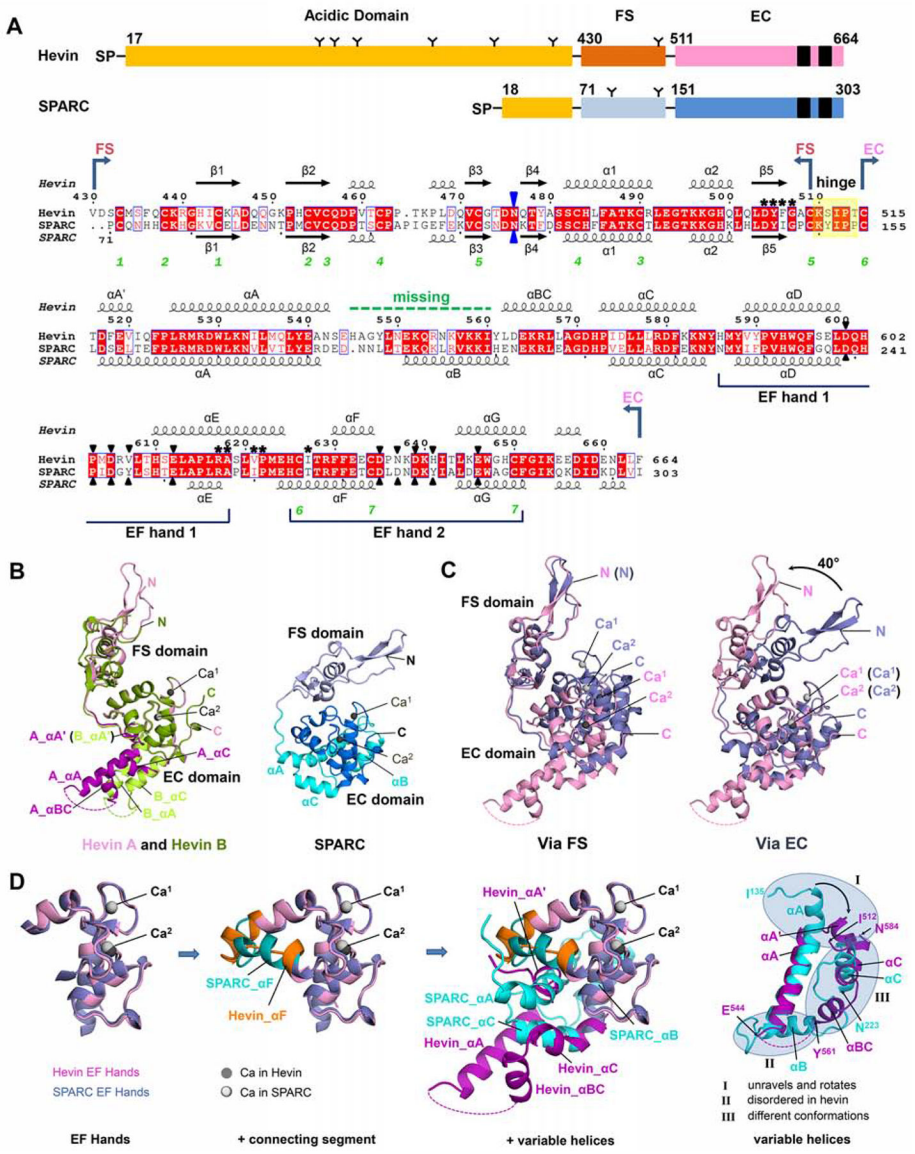

Figure 2. Hevin and SPARC FS-EC tandems are structurally different.

(A) Domain structure of hevin and SPARC (top). EF-hands are indicated with black rectangles, N-linked glycosylation sites with 'Y', and signal peptides with SP. Sequence alignment of the human hevin and human SPARC FS-EC tandems with secondary structure elements indicated (below). Conserved residues are highlighted in red, Ca^{2+}-binding residues are indicated by black triangles, and a conserved N-linked glycosylation site is indicated with a blue triangle. Cysteines participating in disulfide bonds are indicated with numbers 1-7 in green. The hinge between the FS and EC domains is highlighted in yellow. Hevin residues at the FS-EC interface are marked by an asterisk. The region between αA and αBC is disordered in hevin and shown as a dashed green line. In human hevin, the EGF domain spans V^{430}-Q^{457}, and the Kazal domain D^{458}-K^{510}; in mouse hevin, the EGF domain spans A^{416}-Q^{443}, and the Kazal domain D^{444}-K^{496}.

(B) Comparison of hevin and SPARC 3D structures. Superposition of hevin mol A (pink/magenta) and mol B (olive/light green) comprising the asymmetric unit (FS in pink or olive, the rest in magenta or light green) (left). Ca^{2+}-ions in hevin mol A and mol B are shown as dark gray and white spheres, respectively. SPARC (PDB: 1BMO) with FS domain in lavender, EF hands in skyblue, and the remainder in cyan (right). Ca^{2+}-ions in SPARC are shown as dark gray spheres.

(C) Superposition of hevin (pink) and SPARC (slate blue). Superposition using the FS domain (left) and using the EF-hands (right) of the EC domains. Ca^{2+}-ions are shown as dark gray and light gray spheres in hevin and SPARC, respectively.

(D) Comparison of the hevin and SPARC EC subdomain elements. From left to right: EF-hands; EF-hands and their connecting segments (orange or cyan); the EC domains with the 'variable helices' in hevin (magenta) and SPARC (cyan); and superposition of the 'variable helices' in hevin and SPARC.

See also Figures S3 and S4.

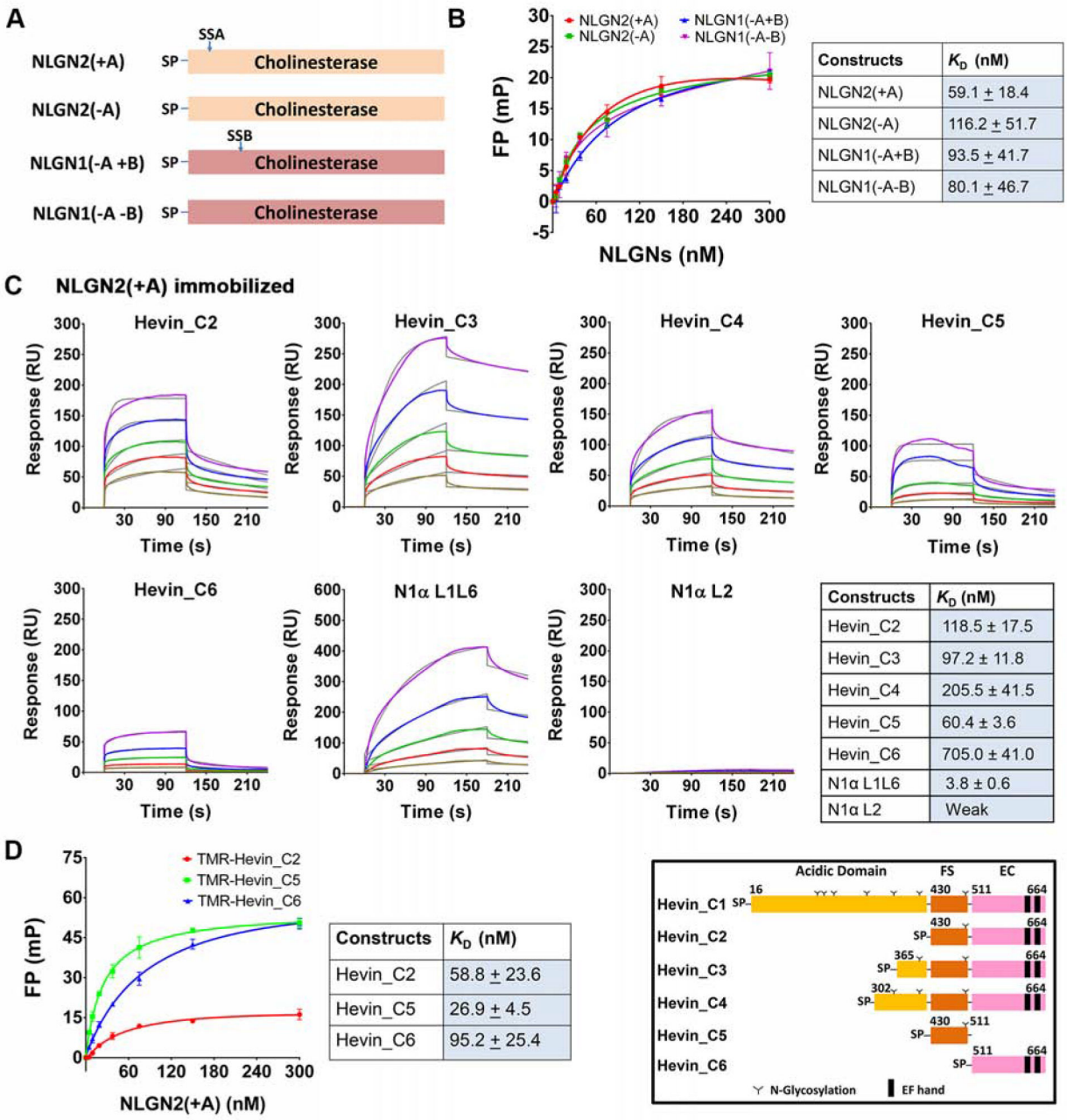

Figure 3. Hevin interacts with NLGNs.

(A) Extracellular domains of NLGN1 and NLGN2 splice forms used in this study. NLGN2 can accommodate splice insert SSA, while NLGN1 can accommodate SSA and/or SSB. SP, signal peptide.

(B) TMR-hevin_C2 (FS-EC tandem) binding to different NLGN splice forms in an FP-assay. Data points represent triplicate measurements with the error bars showing the standard deviations. K_D values were averaged over two independent experiments and the standard deviations given (mean ± SD).

(C) Binding of soluble hevin fragments to an NLGN2(+A)-coupled sensor by SPR using a concentration series of 0, 250, 500, 1000, 2000 and 4000 nM. Binding curves of hevin_C2,

hevin_C3, hevin_C4, hevin_C5, and hevin_C6 were fit to a 1:1 binding model (grey). N1α L1L6 (0–30 nM) was used as a positive control for binding, and n1α L2 (0-50 nM) as a negative control. The K_D values were calculated by averaging K_D values from two independent experiments (mean ± SD).

(D) Comparison of the binding of TMR-hevin_C5 (FS), TMR-hevin_C6 (EC) or TMR-hevin_C2 (FS-EC) to NLGN2(+A) in an FP-assay. Data points represent triplicate measurements with the error bars showing the standard deviations. K_D values were averaged over two independent experiments and the standard deviations given.

Legend (bottom right): hevin constructs used for the binding studies.

See also Figures S1.

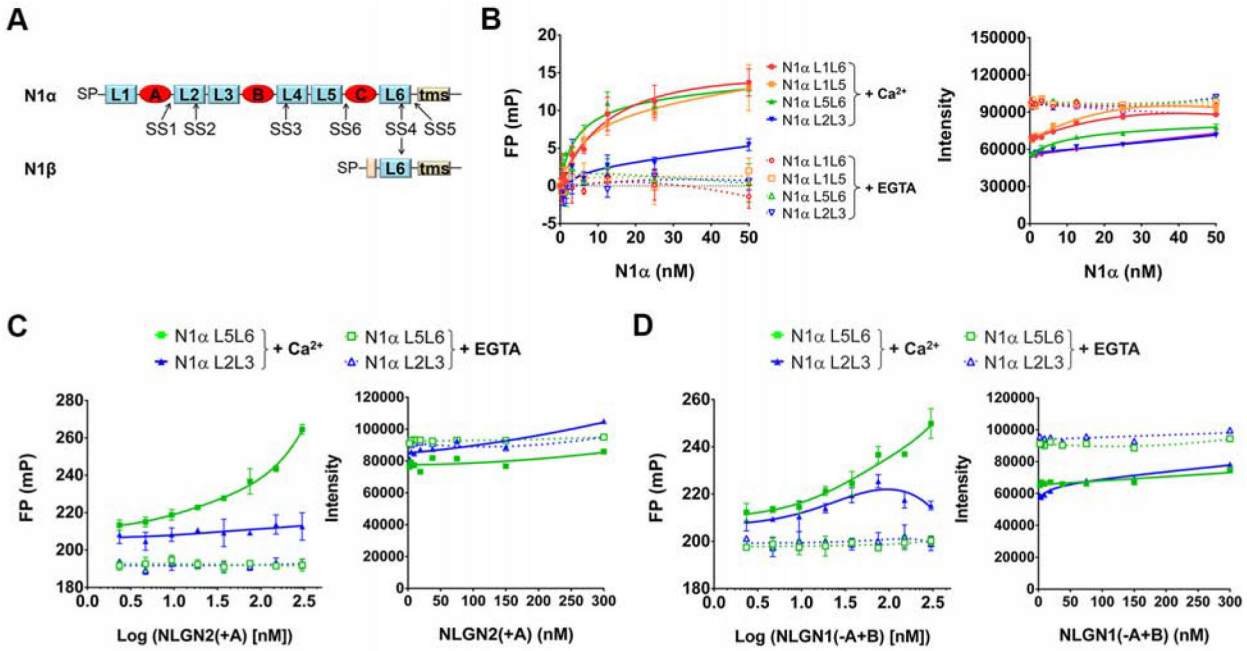

Figure 4. Hevin interacts with neurexin 1α.

(A) Domain structure of neurexin 1α (n1α) and neurexin 1β (n1β). Signal peptides (SP), transmembrane segments (tms), and splice inserts (SS1-SS6) are indicated.

(B) Binding of TMR-hevin_C5(FS) to n1α L1L6 and fragments (n1α L1L5, n1α L5L6, and n1α L2L3) in presence of Ca^{2+} (solid symbols, solid lines) or 10 mM EGTA (open symbols, dotted lines) in an FP-assay. The change in fluorescence polarization is shown on the left, and the total fluorescence intensity to monitor any general increase is shown on the right.

(C) Binding of NLGN2(+A) to TMR-hevin_C5 pre-incubated with n1α L5L6 or n1α L2L3 in presence and absence of Ca^{2+} in an FP-assay.

(D) Binding of NLGN1(−A, +B) to TMR-hevin_C5 pre-incubated with n1α L5L6 or n1α L2L3 in presence and absence of Ca^{2+} in an FP-assay.

Data points in B, C and D represent triplicate measurements with the error bars representing their standard deviations. FP signal shown left, the total fluorescent intensity as a control for spurious increases is shown right. Data presented in B, C and D are representative of at least two independent experiments.

See also Figures S1.

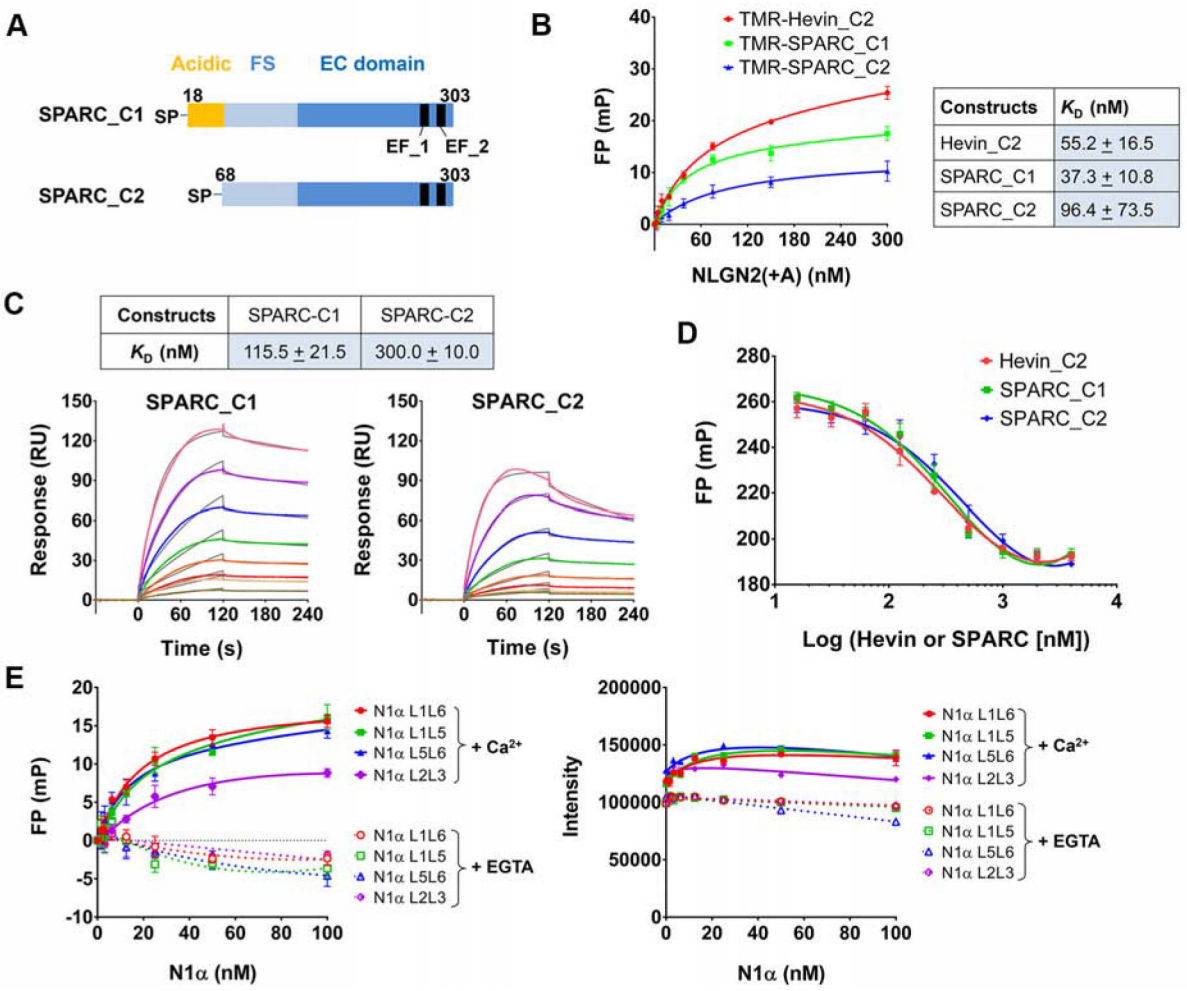

Figure 5. SPARC interacts with NLGNs and neurexin 1α.

(A) Human SPARC constructs used in this study.

(B) Binding of TMR-SPARC_C1, TMR-SPARC_C2, and TMR-hevin_C2 bind to NLGN2(+A) in an FP-assay. The K_D values averaged over two independent experiments with standard deviations are listed. Note: differences in the shape and size between the three proteins, impacting their tumbling properties, likely result in differences in the efficiency of the FP signal.

(C) Binding of SPARC_C1 and SPARC_C2 to an NLGN2(+A)-coupled sensor by SPR using a concentration series of 0, 31.25, 62.5, 125, 250, 500, 1000, 2000, and 4000 nM. Binding curves of SPARC_C1 and SPARC_C2 were fit to a 1:1 binding model (grey). The calculated K_D values averaged over two independent experiments with standard deviations are listed.

(D) Disruption of the TMR-hevin_C5(FS):NLGN2(+A) complex by increasing amounts of unlabeled hevin_C2 (red), SPARC_C1 (green) or SPARC_C2 (blue) in an FP-assay.

(E) TMR-SPARC_C1 binding to n1α L1L6 and fragments (n1α L1L5, n1α L5L6 and n1α L2L3) in presence of Ca^{2+} (solid symbols, solid lines) or 10 mM EGTA (open symbols, dotted lines) in an FP-assay.

Data points in B, D and E represent triplicate measurements with the error bars representing their standard deviations. Data presented here is representative of at least two independent experiments.

See also Figures S1.

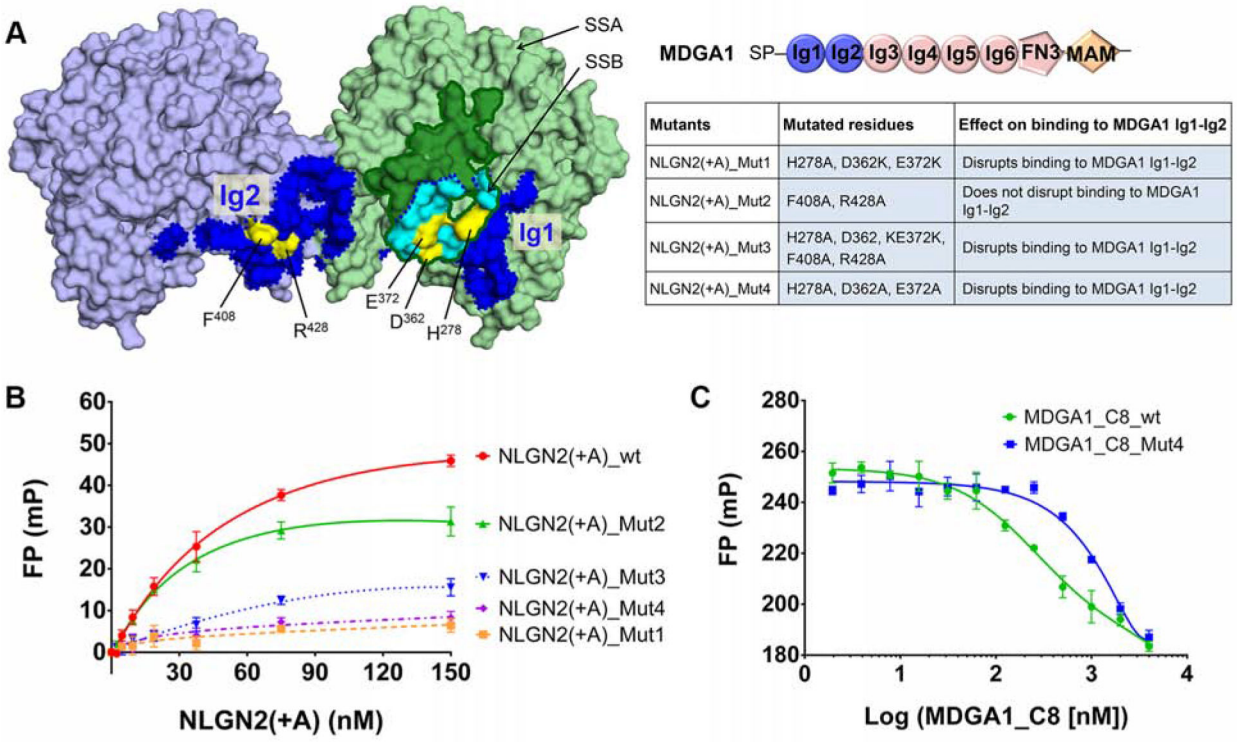

Mutants	Mutated residues	Effect on binding to MDGA1 Ig1-Ig2
NLGN2(+A)_Mut1	H278A, D362K, E372K	Disrupts binding to MDGA1 Ig1-Ig2
NLGN2(+A)_Mut2	F408A, R428A	Does not disrupt binding to MDGA1 Ig1-Ig2
NLGN2(+A)_Mut3	H278A, D362, KE372K, F408A, R428A	Disrupts binding to MDGA1 Ig1-Ig2
NLGN2(+A)_Mut4	H278A, D362A, E372A	Disrupts binding to MDGA1 Ig1-Ig2

Figure 6. Hevin FS domain and MDGA1 Ig1 share overlapping binding sites on NLGN2

(A) Solvent-accessible surface of the NLGN2 dimer (monomers in slate blue and light green; PDB: 5v5v). The MDGA1 Ig1-Ig2 binding site on NLGN2 is shown with dark blue dotted perimeter, the neurexin 1β (n1β) binding site of NLGN1 mapped onto NLGN2 is shown with a dark green dotted perimeter (PDB: 5OJ6). The surface region of NLGN2 that binds both MDGA1 Ig1 and n1β is shown in cyan, while that binding only MDGA1 is shown in dark blue and that binding only n1β is shown in green. Binding sites are defined as residues located within 5 Å of the contacting partner. Domain schematics for MDGAs are shown upper right side, and NLGN2 mutants used in this study are mapped onto the surface in yellow, see table lower right side.

(B) TMR-hevin_C5 (FS) binding to a panel of NLGN2 mutants in an FP-assay.

(C) Disruption of the TMR-hevin_C5(FS):NLGN2 complex by increasing amounts of MDGA1 Ig1-Ig2 (MDGA1_C8; green) or mutant MDGA1 Ig1-Ig2 (MDGA1_C8_Mut4; $R^{105}A$, $Y^{107}A$, $R^{123}A$, $F^{154}A$, $R^{156}A$, $Y^{187}A$; blue) in an FP-based competition study.

Data points in B and C represent triplicates, and error bars indicate their standard deviations. Data presented here is representative of at least two independent experiments.

See also Figures S1.

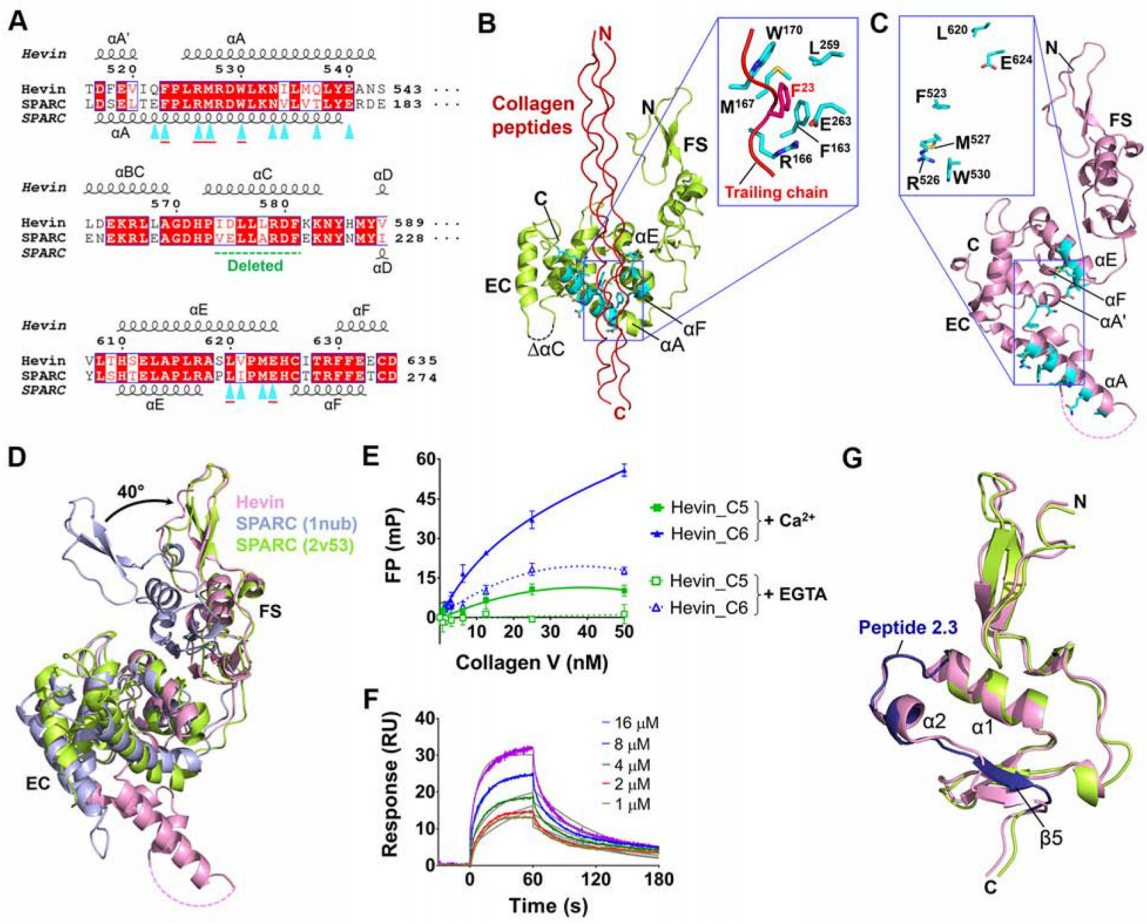

Figure 7. Hevin binds collagen V.

(A) Residues in SPARC that bind a collagen III tri-peptide (interaction distances < 5 Å; PDB: 2v53) are indicated with cyan triangles in a sequence alignment of human hevin and human SPARC; those forming a pocket for collagen III F^{23} (see B) are further underlined in red. A deletion in SPARC activates collagen binding, shown in green (used for PDB: 2v53 and 1nub).

(B) Binding site in SPARC (green/cyan) for a collagen III tri-peptide (red) (PDB: 2v53). A zoom-in shows key residues that form a pocket around F^{23} from the trailing chain of the collagen III tri-peptide, including F^{163}, R^{166}, M^{167}, W^{170}, L^{259} and E^{263} (numbered F^{146}, R^{149}, M^{150}, W^{153}, L^{242} and E^{246} in PDB: 2v53).

(C) Hevin counterpart of the SPARC/collagen-interaction site with corresponding zoom-in.

(D) Superposition of the FS-EC tandem from hevin (pink), the collagen-bound form (green, PDB: 2v53), and the collagen-free form of SPARC (slate blue, PDB: 1nub) using the EC domain.

(E) Interaction of the hevin FS domain (TMR-hevin_C5) or EC domain (TMR-hevin_C6) to human collagen V in presence of 2 mM Ca^{2+} (solid lines) or 10 mM EGTA (dotted lines) in a FP assay. Data points represent triplicates, and error bars indicate their standard deviations. Data presented here is representative of at least two independent experiments.

(F) Binding of the hevin EC domain (hevin_C6) to a human collagen V-coupled sensor by SPR using a concentration series of 0, 1, 2, 4, 8, and 16 μM. Binding curves were fit to a 1:1

binding model (grey). Data presented here is representative of at least two independent experiments.

(G) Comparison of the FS domain from hevin (pink) and SPARC (light green) (PDB: 1nub) with an integrin binding site in SPARC shown in dark blue.

See also Figures S3.

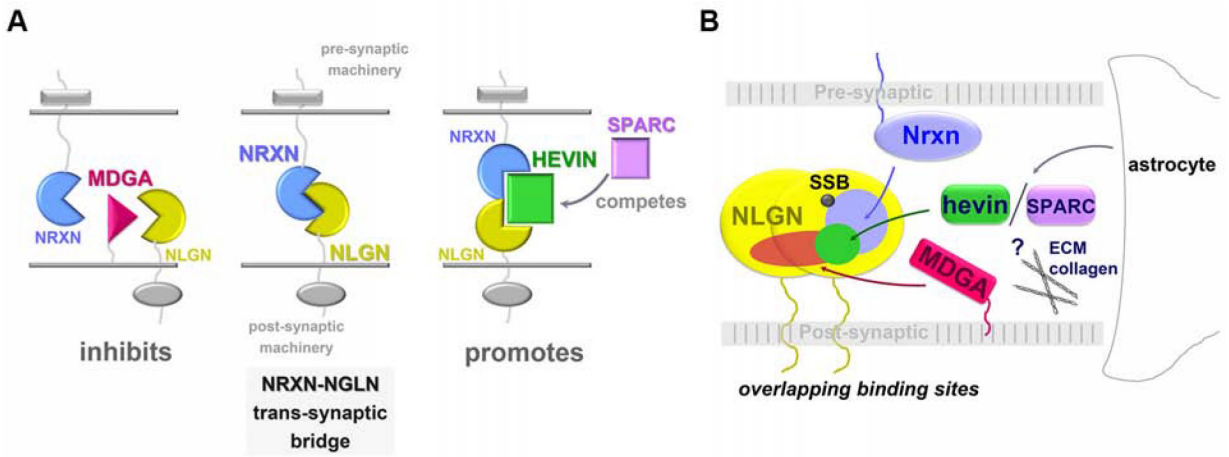

Figure 8. Network of proteins regulating the trans-synaptic neurexin-neuroligin bridge.

(A) Positive and negative regulators of neurexin-neuroligin trans-synaptic bridges.

(B) Regulators of the neurexin-neuroligin trans-synaptic bridge compete for overlapping binding sites. (ECM, extracellular matrix).

Table 1.

Data Collection and Refinement Statistics

Crystal	Native 1	Native 2	Holmium-Derivative
Data Collection			
Wavelength (Å)	1.00001Å	1.00001 Å	1.53532 Å
Space group	$I2_12_12_1$	$I2_12_12_1$	$I2_12_12_1$
Cell dimensions			
a, b, c (Å)	57.66, 132.29, 149.23	57.63, 131.78, 148.62	57.75, 130.97, 148.00
α, β, γ (°)	90, 90, 90	90, 90, 90	90, 90, 90
Resolution (Å)	33.00-2.27 (2.31-2.27)	30.39-2.34 (2.38-2.34)	43.00-3.41 (3.47-3.41)
Mean $I/\sigma(I)$	36.7 (1.9)	40.0 (1.9)	20.9 (1.0)
R_{merge}	0.063 (1.266)	0.062 (1.339)	0.070 (0.889)
R_{pim}	0.019 (0.449)	0.018 (0.490)	0.029 (0.491)
$CC_{1/2}$	0.998 (0.696)	0.979 (0.672)	0.972 (0.637)
Unique reflections	26,686 (1,309)	23,942 (1191)	7865 (322)
Completeness (%)	99.8 (99.1)	99.9 (100.0)	98.5 (85.2)
Multiplicity	12.7 (7.9)	12.1 (8.3)	6.7 (3.3)
Phasing			
Resolution (Å)	-	43.00 - 3.41	
Number of sites	-	5	
Bayes CC	-	49.7 ± 18.3	
Figure of merit	-	0.300	
Refinement			
Resolution (Å)	33.00-2.27 (2.36-2.27)		
R_{work}/R_{free}	18.85/24.07 (22.75/31.33)		
Reflections used R_{work}/R_{free}	25,958/1298 (2098/110)		
Non-hydrogen atoms	3,636		
Protein	3,403		
Water	155		
Other	78		
B factors (Å^2), overall	42.2		
Protein	42.3		
Water	37.9		
Other	50.4		
r.m.s. deviations			
bond lengths (Å)	0.009		
bond angles (°)	1.09		
Ramachandran plot (%)			
Favored	97.3		
Allowed	2.7		
disallowed	0.0		

Crystal	Native 1	Native 2	Holmium-Derivative
Rotamer outliers, n (%)	1 (0.27)		

KEY RESOURCES TABLE

REAGENT or RESOURCE	SOURCE	IDENTIFIER
Chemicals, Peptides, and Recombinant Proteins		
Leupeptin	VWR Amresco	Cat# J580
Pepstatin	VWR Amresco	Cat# J583
Phenylmethylsulfonyl fluoride	Sigma	Cat# P7626
Ni-NTA Agarose	Invitrogen	Cat# R901-15
Glutathione Sepharose 4B	Bioworld	Cat# 20182003-2
HEPES	Sigma	Cat# H3375
OneQuant TAMRA (5/6)SE	G Biosciences	Cat# 786-079
Dimethyl sulfoxide	Sigma	Cat# D8418
Gel Filtration Markers Kit	Sigma	Cat# MWGF200
Amine Coupling Kit	GE Healthcare	Cat# BR-1000-50
HBS-N buffer, 10x	GE Healthcare	Cat# BR-1006-70
Tween-20	Fisher Scientific	Cat# BP337
DSSO	Thermo Fisher	Cat# A33545
SpinOUT GT-600, 3ml Column	G Biosciences	Cat# 786-171
Fluorescence Polarization Assay Plate	Corning	Cat# 3991
Triton X-100	Sigma	Cat# T9284
EDTA	Sigma	Cat# E5134
EGTA	Sigma	Cat# E4378
Calcium chloride dihydrate	Sigma	Cat# C5080
Surfactant P20	GE Healthcare	Cat# BR100054
Polyethylene glycol 3350	Hampton Research	Cat# HR2-605
Sodium acetate	Sigma	Cat# S7545
Sodium formate	Sigma	Cat# 71539
Glycerol	Invitrogen	Cat# 15514-011
Holmium (III) chloride hexahydrate	Alfa Aesar	Cat# 11277
Human Collagen Type V	Sigma	Cat# CC077
Deposited Data		
Hevin FS-EC	This paper	PDB ID: 7KBU
SPARC FS-EC	Hohenester et al., 1997	PDB ID: 1BMO
SPARC-collagen complex	Hohenester et al., 2008	PDB ID: 2V53
Helix C deletion mutant of SPARC FS-EC	Sasaki et al., 1998	PDB ID: 1NUB
Complex of NLGN2 with MDGA1 Ig1-Ig2	Gangwar et al., 2017	PDB ID: 5V5V
Complex of NLGN1 with MDGA1 ectodomain	Elegheert et al., 2017	PDB ID: 5OJ6
Experimental Models: Cell Lines		
HighFive Cells	ThermoFisher Scientific	Cat# B85502
Experimental Models: Organisms/Strains		
Escherichia coli BL21(DE3)	Novagen	Cat# 69450-3
Recombinant DNA		

REAGENT or RESOURCE	SOURCE	IDENTIFIER
Human hevin cloned in the pfastbac Vector	This paper	GenBank:BC033721
Human SPARC cloned in the pfastbac Vector	This paper	GenBank:NM_003118
Rat Neuroligin 2 cloned in the pfastbac Vector	Gangwar et al., 2017	GenBank:NM_053992
Human Neuroligin 1 cloned in the pfastbac Vector	Gangwar et al., 2017	GenBank:BC032555
Bovine Neurexin 1α L1L6 cloned in the pfastbac Vector	Chen et al., 2011	GenBank:NM_174404
Bovine Neurexin 1α L5L6 cloned in the pfastbac Vector	Chen et al., 2011	GenBank:NM_174404
Bovine Neurexin 1α L1L5 cloned in the pfastbac Vector	Lu et al., 2014	GenBank:NM_174404
Bovine Neurexin 1α L2 cloned in the PGEX Vector	Sheckler et al., 2006	GenBank:NM_174404
Bovine Neurexin 1α L2L3 cloned in the PGEX Vector	Liu et al., 2018	GenBank:NM_174404
Software and Algorithms		
Prism 6	GraphPad Software	https://www.graphpad.com/scientific-software/prism/
SEDNTERP	Laue et al., 1992	https://www.sednterp.unh.edu/
SEDFIT	Schuck, 2000	http://www.analyticalultracentrifugation.com/default.htm
Gussi 1.0.8	Brautigam, 2015	https://www.utsouthwestern.edu/labs/mbr/assets/README.txt
HKL2000	Otwinowski and Minor,1997	https://www.hkl-xray.com/
Pymol	Schrödinger, LLC.	http://www.pymol.org
PHENIX	Liebschner et al., 2019	https://www.phenix-online.org/
STRIDE	Frishman and Argos, 1995	http://webclu.bio.wzw.tum.de/stride/
Gesamt	Krissinel, 2012	http://ccp4serv7.rc-harwell.ac.uk/gesamt/
Clustal Omega	Sievers et al, 2011	https://www.ebi.ac.uk/Tools/msa/clustalo/
ESPript 3.0	Robert and Gouet et al, 2014	http://espript.ibcp.fr/ESPript/ESPript/
CCP4	Winn et al, 2011	http://www.ccp4.ac.uk/
COOT	Emsley et al., 2010	http://www2.mrc-lmb.cam.ac.uk/Personal/pemsley/coot
PBDe PISA	Krissinel and Henrick, 2007	http://www.ebi.ac.uk/pdbe/pisa/
Other		
Insect Express with L-Glutamine medium	Lonza	Cat# 12-730Q
Mono Q 5/50 GL	GE Healthcare	Cat# 17-5166-01
HiLoad 16/60 Superdex 200 pg	GE Healthcare	Cat# 28-9893-35
Superdex 200 Increase 3.2/300	GE Healthcare	Cat# 28-9909-46
Sensor Chip C1	GE Healthcare	Cat# BR-1005-35
Sensor Chip CM5	GE Healthcare	Cat# BR-1000-12